Resilience Analytics for Integrated Power and District Heating Networks by Identifying Critical Contingencies

Morteza Zare Oskouei, Tayfur Gökçek, Ayşe Kübra Erenoğlu, *Senior Member, IEEE*, Ozan Erdinç, *Senior Member, IEEE*, and João P. S. Catalão, *Fellow, IEEE*.

***Abstract*—The increasing structural and operational interdependencies between power distribution networks (PDNs) and district heating networks (DHNs) have intensified the need for integrated and resilient contingency management strategies. This necessitates the development of advanced analytical frameworks for probabilistic N-1 and N-k security assessments that capture the temporal and spatial coupling of these networks throughout all phases of resilient operations. Owing to this necessity, this paper proposes a novel contingency multi-criteria assessment framework to quantify the interdependencies between the resilience of PDNs and DHNs, incorporating various phases of contingency chains. The methodology utilizes the Simultaneous Evaluation of Criteria and Alternatives (SECA) approach to systematically rank critical contingencies, thereby revealing the most severe potential cascading failures that threaten energy security. The following stage entails the presentation of a pioneering spatio-temporal cascading failure analytical model, which is developed to coordinate the withstand-and-recover phases across interdependent PDNs and DHNs. This model is supported by tailored operational resilience key performance indicators (KPIs) that trace power-induced heating service degradation across diverse backup configurations, including line-pack storage, energy storage systems, and integrated demand response programs. As another unattainable novelty, the developed decision-making framework integrates static and dynamic resilience analyses to provide an all-encompassing comprehension of the integrated PDNs and DHNs resilience. The proposed framework is validated through co-simulation of a modified IEEE 33-bus PDN and a 32-node DHN, employing analytical and empirical methodologies. The results indicate that the strategic implementation of backup flexibility resources, when synchronized with DHN service provision, can enhance DHN service continuity by up to 29%, while concurrently reducing the full recovery time by nearly 41%. Dynamic resilience analyses are further conducted in DIgSILENT PowerFactory to evaluate the real-time transient response under top-ranked contingency scenarios.**

***Index Terms*—Contingency multi-criteria decision-making assessment, data-driven prioritization, static and dynamic outage analysis, power-heat nexus, resilience key performance indicators (KPI).**

NOMENCLATURE

Set and indexes

$\mathcal{G}$	Set of PtH units, indexed by *g*.
$\mathcal{I}$	Set of PDN buses, indexed by *i, j*.
$\mathcal{L}$	Set of power feeders, indexed by *l*.
$\mathcal{N}$	Set of nodes in DHNs, indexed by *n, o*.
$\mathcal{P}$	Set of pipelines in DHNs, indexed by *p*.
$\mathcal{S}$	Set of contingencies, indexed by *s*.
$\mathcal{T}$	Set of dispatch intervals, indexed by *t*.
$\mathcal{U}$	Set of CHP units, indexed by *u*.
$\mathcal{L}_s$	Subset of outage power feeders in contingency scenario *s*.
Λ_n^{P-}, Λ_n^{P+}	Subset of pipelines ending/starting at node *n*.

Constants

g_{ij}^y, b_{ij}^y	Real and imaginary segments of admittance matrix of power distribution grid.
$ENS_i^{p(\cdot)}$, $ENS_n^{h(\cdot)}$	Value of lost critical and non-critical electric and and heating demands.
$\widehat{H_{n,t}^D}$, $\widetilde{H_{n,t}^D}$	Critical and non-critical heat demands of heat exchanging station at time slots *t*.
$\widehat{P_{i,t}^D}$, $\widetilde{P_{i,t}^D}$	Critical and non-critical active electrical demands at bus *i* at time slots *t*.
$T_{p,t}^{am}$	Ambient temperature of pipeline *p* at time slots *t*.
$\dot{m}_n^{(\cdot)}$, $\dot{m}_p$	Mass flow rate of source/load/pipelines.
ρ	Specific heat capacity of water.
λ_p	Heat transfer coefficient of pipe *p*.
κ_p	Length of pipe *p*.

Variables

$H_{n,t,s}^{TS,dis}$, $H_{n,t,s}^{TS,ch}$	Heat released and drawn by TESSs during time *t* of failure scenario *s*.
$H_{n,t,s}^{PtH}$	Thermal output of PtH units at node *n* during time *t* of failure scenario *s*.
$H_{n,t,s}^{Z}$	Generation of heat source at node *n* during time *t* of failure scenario *s*.
$P_{u,t,s}^{CHP}$, $H_{u,t,s}^{CHP}$	Electric/thermal power output of CHP unit during time *t* of failure scenario *s*.
$P_{i,t,s}^{ES,dis}$, $P_{i,t,s}^{ES,ch}$	Power released and drawn by BESSs at bus *i* during time *t* of failure scenario *s*.
$P_{g,t,s}^{PtH}$	Power consumption of PtH units during time *t* of failure scenario *s*.
$P_{i,t,s}^{inj}$, $Q_{i,t,s}^{inj}$	Active/reactive power injection at bus *i* during time *t* of failure scenario *s*.
$P_{i,t,s}^{WT}$, $Q_{i,t,s}^{WT}$	Actual active/reactive power output of wind turbine at bus *i* during time *t* of failure scenario *s*.
$P_{i,t,s}^{PV}$	Actual power output of PV systems at bus *i* during time *t* of failure scenario *s*.
$S_{l,t,s}$, $P_{l,t,s}$, $Q_{l,t,s}$	Apparent/active/reactive power flow through power distribution feeder *l* at time *t* of failure scenario *s*.
$SoC_{i,t,s}^{ES}$	Scheduled state-of-charge of ESSs.
$v_{i,t,s}$, $\theta_{i,t,s}$	RMS voltage magnitude and phase angle of bus *i* during failure scenario *s*.
$\tau s_{p,t,s}^{ou}$, $\tau s_{p,t,s}^{in}$	Outlet/inlet temperature of mass flow in pipeline *p* of supply network during time *t* of failure scenario *s*.
$\tau r_{p,t,s}^{ou}$, $\tau r_{p,t,s}^{in}$	Outlet/inlet temperature of mass flow in pipeline *p* of return network during time *t* of failure scenario *s*.
$\tau s_{n,t,s}^{mix}$, $\tau r_{n,t,s}^{mix}$	Mixture temperature at confluence node.
$\tau s_{n,t,s}^{(\cdot)}$, $\tau r_{n,t,s}^{(\cdot)}$	Supply/return temperature of heat source and exchanger at node *n*.
$\beta_{f,u,t,s}$	f^{th} operation corner point of CHP unit *u* during time *t* of failure scenario *s*.
$\gamma_{i,t,s}^{P}$, $\gamma_{n,t,s}^{H}$	Ratio of electric and thermal power served during failure scenario *s*.
$\Delta(\cdot)_{i,t,s}^{IDR}$	Electric and heat demands withdrawal for DRP implementation.

I. INTRODUCTION

In the context of urban infrastructures undergoing a transition toward smart, low-carbon, and interconnected energy ecosystems, the operational interplay between power distribution networks (PDNs) and district heating networks

M. Zare Oskouei is with the Faculty of Electrical and Computer Engineering, Sahand University of Technology, Tabriz, Iran, and also with Department of Electrical Engineering, Yildiz Technical University, Istanbul 34349, Turkiye (e-mail: m.zare@sut.ac.ir). T. Gökçek is with the Clean Energy Technologies Institute, Yildiz Technical University, Istanbul 34220, Turkiye. A.K. Erenoğlu is with the Department of Electrical Engineering, and also with the Clean Energy Technologies Institute, Yildiz Technical University, Istanbul 34220, Turkiye. O. Erdinç is with the Department of Electrical Engineering, Yildiz Technical University, Istanbul 34349, Turkiye, and also with the Faculty of Engineering, University of Porto, Porto, Portugal. J.P.S. Catalão is with the Research Center for Systems and Technologies (SYSTEC), Advanced Production and Intelligent Systems Associate Laboratory (ARISE), Faculty of Engineering, University of Porto, 4200-465 Porto, Portugal.

(DHNs) emerges as a strategic cornerstone of sustainable development, underscoring the imperative for integrated, holistic approaches to energy infrastructure planning and management [1]. The interdependence between PDNs and DHNs has the potential to result in enhanced efficiency, reduced operational costs, and a decrease in emissions relative to the operation of individual networks operating independently [2]. Nevertheless, the coupling between heterogeneous energy systems presents a paradoxical situation with regard to the requirements of economic operation and resiliency, as this interdependence increases the vulnerabilities of these systems to outages, which in turn can cascade from PDNs into DHNs. Addressing this issue necessitates a comprehensive framework that extends beyond conventional resiliency metrics and incorporates cross-domain dynamics and interdependency effects.

A. Motivation and literature review

The integration of PDNs and DHNs requires layer-by-layer management to ensure energy flexibility and resilience in the face of multifaceted disturbances. The power systems infrastructure is susceptible to a multitude of faults resulting from external shocks, which can subsequently lead to cascading failures in DHNs that are fed by power-to-heat (PtH) units. Furthermore, the resilience challenges of interdependent PDNs and DHNs may be further complicated by various factors, such as conflicts between electrical and heat load restoration under limited supply capacity, the existence of multiple uncertain parameters, and the thermal dynamics of the DHNs [3]. To illustrate the aforementioned vulnerabilities, one may cite the cyber-attack on the Ukrainian power grid in 2019, which resulted in widespread power outages that affected the heating services during the winter season [4]. It is therefore of the utmost importance to identify critical contingencies in integrated energy systems and to take preventive measures for system design and resilient operation to maintain service continuity. These limitations collectively underline a fundamental research gap in the resilience assessment of integrated energy systems, particularly the lack of quantifiable, interdependent, and temporally dynamic performance indicators that can holistically capture the cross-domain effects of disruptions across power and heat infrastructures.

Despite the well-documented vulnerabilities of PDNs and DHNs infrastructure, resilience-enhancing measures are based on criteria that treat these networks as independent entities, thereby ignoring the impact of their interdependent operation. The most commonly employed and operationally effective strategies to enhance the resilience of integrated PDNs and DHNs encompass a range of approaches, including power distribution line hardening, multi-carrier microgrid formation and operation for self-healing purposes, the utilization of distributed resources such as energy storage systems (ESSs) and renewable energy sources (RESs) for local load restoration, and grid reconfiguration to minimize load shedding ratios during the recovery phase [5], [6]. For instance, Yan *et al.* [7] developed a coordination model for the regional-district integrated energy systems. The model was a robust framework consisting of a tri-level two-stage structure designed to effectively manage random outages. The proposed tri-level model for integrated PDNs and DHNs in [8] was regarded as a risk-averse approach to enhancing load restoration in the event of uncertainties. The aforementioned model, which integrated network reconfiguration and mass flow rate control, was formulated as a risk-constrained mixed-integer program and solved via a nested C&CG algorithm. Zhou *et al.* [9] presented a two-stage robust model for the resilient operation of integrated PDNs and DHNs in the case of extreme weather events, which considered both the moment and the Wasserstein metric information, however, they rarely provide spatially distributed resilience metrics or post-contingency recovery insights. In [10], a preparedness analysis of the interdependent energy systems was conducted in the context of extreme weather events, employing data-based models to assess the impact of component failures. Lu *et al.* [11] proposed a bi-objective distributionally robust chance-constrained approach for the integrated electrical and heat load restoration process, which considered the uncertainty in renewable power generation and outdoor temperature. The optimal sizing of the multi-carrier energy system, along with the implementation of an energy management strategy based on a time-of-use demand response program (DRP), was presented in [12] to evaluate the resilience of the energy system under different seasonal conditions. A reconfiguration method for integrated PDNs and DHNs was developed in [13] to enhance resilience in the event of natural disasters. Additionally, the method facilitated the restoration of short-term faults by regulating the switches in PDNs and the valves in DHNs for the purpose of ensuring human safety. Zhou *et al.* [14] proposed a resilience-oriented planning model for integrated electricity and heat systems based on a distributionally robust optimization framework, taking into account uncertainty in extreme events and the outage. In [15], the resilience of integrated energy systems was analyzed from two vantage points, system-wide and component-wide. That study also sought to quantify the impacts of extreme natural disasters. An integrated energy system resilience assessment framework was developed in [16], which was considered a multi-stage cascading fault and recovery process under outages to evaluate sector-coupled energy systems interdependency. Moreover, a novel graph theory integrating the radiality constraint model and the post-disturbance model was proposed in [17] with the objective of enhancing resilience in the context of diverse reconfiguration scenarios.

Despite the growing attention to resilience in integrated energy systems, previous resilience assessment methodologies have conspicuously omitted probabilistic screening of critical N-1 and N-k contingencies. These contingencies are indispensable for pinpointing the most impactful failure scenarios in complex networks. Moreover, extant studies predominantly fail to quantify the integrated energy systems' resilience across both spatial and temporal dimensions, considering the cascading dynamics and feedback loops within interdependent energy systems. A salient issue that has been overlooked in extant literature pertains to the investigation of the temporal dynamic factors in integrated energy systems under critical conditions that play an essential role in these systems, including the mutual resilience sensitivity rate, long-term stabilization phases, and immediate post-contingency responses. Furthermore, all of the studies that have been conducted thus far demonstrate a correlation between the resilience level of interconnected PDNs and DHNs and the demand that is supplied during and after an event, with this latter factor being assessed using either a triangle or a trapezoid performance curve. Nevertheless, these performance curves assess PDNs and DHNs as isolated entities, failing to adequately address the interconnectivity and cascading implications between these entities. Therefore, there is a lack of quantifiable mechanisms to assess the interdependence between the resilience of PDNs and DHNs during the response and recovery after disasters, which are crucial instruments for identifying vulnerabilities affecting the infrastructures during high-impact low-probability (HILP) events. Table I presents a comparative analysis of the features of previous integrated PDNs and DHNs resilience assessment approaches as they pertain to the strategy discussed in this study.

B. Technical contribution and paper structure

This study advances the field through the provision of a robust cascading failure analytics framework for the assessment and enhancement of the resilience of interdependent

TABLE I
COMPARATIVE ANALYSIS OF RELATED WORKS IN RESILIENCE ANALYTICS OF INTEGRATED PDNS–DHNS

Ref.	Critical contingency identification	Spatio-temporal resilience modeling	Interdependency quantification	Hybrid static–dynamic analysis
[9]	×	✓ (pre-outage)	✓ (limited)	×
[10], [11]	×	×	✓ (limited)	×
[14]	×	×	×	×
[16]	×	✓ (analytics)	✓	×
Our study	✓ (SECA-based N-1/N-k)	✓ (spatio-temporal KPIs)	✓ (explicit cascading modeling)	✓ (RMS-based simulation)

PDNs and DHNs, addressing both static and dynamic aspects of system resiliency and response in critical contingencies. Our work transcends conventional methodological approaches, pioneering a sophisticated interplay of advanced analytics and dynamic simulations to address the pressing challenges of modern energy systems. This paper is not just a theoretical study; rather, it is a manifesto of technological evolution and resilience engineering. The groundbreaking contributions and attributes of this paper are delineated as follows:

1) *Critical Contingency Identification via SECA-based Multi-Criteria Analysis:* We develop an avant-garde strategy that leverages the simultaneous evaluation of criteria and alternatives (SECA) approach to identify the critical PDN feeders, which are the main arteries of integrated energy networks. This is the first study that integrates SECA-based screening with cascading resilience analytics in PDN-DHN systems. This data-driven approach meticulously evaluates operational and energy security criteria to pinpoint critical N-1 and N-k contingencies with unparalleled precision, which threaten the stability and resiliency of integrated PDNs and DHNs. The distinctive feature of this study is that the resilience assessment does not focus on a singular scenario but instead encompasses the impacts of a multitude of critical scenarios, which depict the diverse responses of the integrated energy system.
2) *Integrated Cascading Failure Analytics Framework for Interdependent Energy Systems:* We develop a cascading failure analytics framework to quantify the cascading impact of power outages on the ability of DHN to survive both critical and noncritical demands, which emulate the effects of determined critical contingency scenarios. To the best of the authors' knowledge, this is the first attempt that quantifies the interdependence between the resilience of power and heat infrastructures by tracking how the PDN response during N-1 or N-k outages is cascaded into the DHN operation. It is fair to say that this is the first attempt to coordinate the optimal exploitation of line pack storage capacity of gas pipelines, integrated DRP, and ESSs to address the hitherto unacknowledged interdependence between the resilience of the PDN and DHN by designing more sophisticated analytical layers for the cascading failure model.
3) *Development of Interdependent Resilience KPIs for PDN-DHN Systems:* We propose a novel set of resilience key performance indicators (KPIs) that quantify the intricate interdependencies between PDNs and DHNs. These KPIs provide a nuanced understanding of the DHNs' resilience dependency to PDNs in terms of degradation, sensitivity, total loss of service, and recovery trajectory. These metrics are a testament to the depth of our analysis, enabling precise identification of vulnerabilities and the efficacy of resilience-enhancing measures. It is anticipated that the implementation of these KPIs will prompt distribution system operators to transition from isolated and independent operations to a robust scheduling framework.
4) *Hybrid Static–Dynamic Resilience Assessment using RMS Simulations:* We integrate static and dynamic resilience analyses to provide a comprehensive understanding of the integrated PDNs and DHNs resilience. The static analysis identifies critical points and potential vulnerabilities in response to predefined contingency scenarios, while the dynamic analysis evaluates the real-time stability, voltage regulation, and response time of the system using RMS simulations in the DIgSILENT PowerFactory software. This integrated approach is of significant importance to industrial stakeholders and distribution system operators, as it provides a comprehensive technical vision for the development and enhancement of integrated energy systems.

The remainder of this paper is organized as follows. Section II describes the cascading effect of PDN disruptions on the resilient operation of DHNs. Section III is devoted to formulating the proposed resilience KPIs. The simulation results are presented in Section IV. Finally, conclusions and future work are drawn in Section V.

II. DECISION-SUPPORT FRAMEWORK FOR OUTAGE RESILIENCE IN INTEGRATED PDNS AND DHNS

Contemporary energy distribution systems are increasingly marked by profound interdependencies among power, thermal, and gas infrastructures. These interconnections render the system susceptible to complex cascading failures, wherein an external shock in one domain, such as a power feeder outage or gas supply disruption, can propagate and jeopardize the operation of both DHNs and PDNs. To address this, the present work proposes a comprehensive and modular decision-support framework designed to assess and enhance the resilience of integrated PDNs and DHNs in the face of critical contingencies. The proposed framework is comprised of three interconnected layers: (i) contingency anticipation; (ii) failure propagation analysis, which evaluates the cascading effects of power feeder and CHP/PtH outages on both power and heat supply using time-step-based simulation; and (iii) static and dynamic resilience enhancement scheduling, which optimally leverages local distributed energy resources, line pack capacity in gas networks, and responsive consumption-chain management to mitigate disruptions and maintain service continuity.

Let's introduce a typical topology of interdependent PDNs and DHNs consisting of various infrastructures, e.g., wind turbines, PV systems, battery energy storage systems (BESSs), and thermal energy storage systems (TESSs). In the framework of this sustainable energy society, the PDN and DHN are predominantly coupled by PtH units, while, the natural gas network plays a pivotal role in the supply of fuel to centralized CHP units, which are utilized for the generation of both power and heat. Hence, the energy supply for DHNs is achieved through PDNs and gas infrastructure. Therefore, access to reliable energy sources is critical to operating energy-intensive processes in DHNs. External shocks such as natural disasters and cyber-attacks can cause simultaneous disruptions in power feeders, followed by PtH units. To ensure safety, gas production platforms are shut down during the event, which in turn leads to the shutdown of CHP, resulting in widespread disruption in the operation of DHNs. A key feature of the second layer lies in the explicit modeling of the dynamic interaction between networks, which is captured through coupled balance equations at each simulation step. For clarity, an interruption in feeders can impede the adaptability of PDN, consequently leading to the curtailment of PtH operations. This, in turn, results in an elevated degree of reliance on CHP. Subsequently, the depletion of line pack capacity serves as a catalyst for CHP disconnection. This further exacerbates power and heat shortages, thus engendering a two-sided propagation path of failures. This formulation enables quantifiable tracking of cascading effects across infrastructures, ensuring

that the resilience indices reflect the full extent of cross-domain interdependencies. Fig. 1 illustrates the conditions that integrated PDNs and DHNs may experience during successive time steps, including during the occurrence of contingencies and after the clearing of contingencies. By adhering to each of these time steps, this paper aims to achieve global optimal set-points by utilizing resiliency from local generation sources and controllable consumers.

Collectively, the proposed framework furnishes system operators with a data-driven, context-sensitive platform to foresee, absorb, and recover from disruptive events in an optimal and informed manner. The decision-making framework for implementing the developed resilience analytics model is described in Fig. 2. In the first layer, the critical N-1 and N-k contingencies on PDN feeders are identified in the context of integrated energy networks. For this purpose, the SECA method is employed to systematically determine the most critical contingency scenarios that may contain single (N-1 mode) or multiple (N-k mode) outages, to investigate cascading failures in interdependent PDNs and DHNs. Then, the developed structure conducts a failure analysis to determine the necessary actions for the PDN operator to minimize electrical load shedding and maintain the PtH units' operation without compromising the PDN's security. The proposed failure model determines the cascading effects of PDN feeders' outage under each critical scenario on the operation of the DHNs in terms of heat shortage caused by PtH units' failure. It is important to note that the effect of the interruption of production of CHP units, due to disruption in gas facilities following the occurrence of external shocks, on the resilience performance of both PDNs and DHNs is evaluated with respect to the line pack capacity. To enhance the resilience of integrated energy networks to deal with critical scenarios and mitigate the effects of cascading failures on critical consumers, distribution system operators can take various supportive actions. These include optimizing the capacity of distributed generation resources, e.g., RESs and ESSs, utilizing line pack storage capability, and unlocking the flexible potential of controllable loads through integrated DRPs. Integrated DRPs prioritize the restoration of critical loads over non-critical ones, minimizing downtime and enhancing the overall resilience of the system. This approach can lead to measurable improvements in resilience KPIs, such as system recovery and response time to contingencies, demonstrating the effectiveness of integrated energy networks in withstanding adverse contingencies. These KPIs identify the temporal dependencies of PDNs and DHNs in the stages of integrated energy networks degradation and recovery, as well as the spatial characteristics associated with failure location and energy curtailments. Continuous monitoring and analysis of resilience KPIs enable stakeholders to objectively evaluate the effectiveness of proactive measures over time. This iterative process supports ongoing improvements and ensures that the network remains resilient in the face of evolving challenges and threats.

A salient distinguishing attribute of this framework is its capacity to facilitate a seamless integration between steady-state outage analysis and dynamic response validation. This approach enables precise real-time stress testing of PDNs under critical contingency sets, thereby ensuring operational feasibility in terms of grid security margins. It is imperative to acknowledge that the primary factor in the incorporation of resilience considerations in interdependent PDNs and DHNs is the dynamic characteristics of PDNs. Therefore, it is essential to conduct dynamic resilience studies of PDNs for the practical implementation of the developed cascading failure analysis model to optimize stressful conditions to reassure industrial stakeholders. For this purpose, the dynamic state analysis of the PDNs is conducted using the RMS simulation using the DIgSILENT PowerFactory software under the determined critical contingency scenarios to ensure

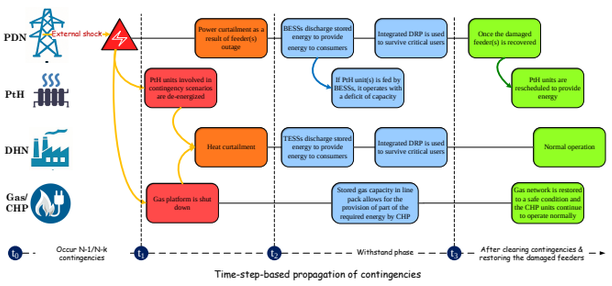

Fig. 1. A chain of actions encountered by interdependent PDNs and DHNs in chronological order under the proposed contingency multi-criteria assessment framework.

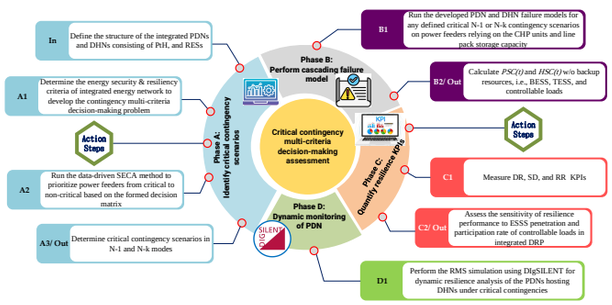

Fig. 2. Conceptual diagram of the proposed contingency multi-criteria decision-making assessment of interdependent PDNs and DHNs.

that local energy balancing strategies do not compromise voltage stability and operational security within the PDN. The proposed critical contingency multi-criteria decision-making assessment framework is exactly what we believe distribution system operators may emulate to reconsider the resilience requirements of integrated energy networks in coordinated operations with local energy prosumers, with the aim of implementing islanding maneuver scenarios in real-time sessions.

Before providing the failure analysis strategy, the key considerations and assumptions made in this study are outlined as follows:

A1. The PDN and DHN are modeled as the balanced radial networks. Dealing with resilience requirements in radial networks is considered to be the most challenging situation due to the unidirectional power flow.

A2. The DHN is assumed to operate under the constant flow and variable temperature (CF-VT) control strategy.

A3. It is commonly assumed that DHNs are resistant to external shocks, including hurricanes and anthropogenic hazards, due to the fact that pipelines are installed underground.

A4. It is assumed that any damaged feeders can be repaired and operated again during the remaining periods of the day under study.

The aforementioned assumptions have been adopted for the purpose of establishing a modeling framework that is both technically feasible and analytically tractable. This framework is designed to isolate the core resilience dynamics of interdependent PDN-DHN systems. These assumptions are widely accepted as standard configurations within the domain of urban PDNs and DHNs. The ramifications and constraints of these assumptions are further delineated in sub-section IV-C.

A. Identification of critical contingency scenarios using data-driven decision making

In the realm of integrated energy networks, where techno-security considerations shape resilient-oriented decisions and policies, SECA's evaluation of multiple criteria provides a more accurate representation of decision-making landscapes. The SECA approach provides a structured and data-driven methodology for identifying and ranking critical contingencies in integrated PDNs and DHNs, thereby supporting effective decision-making to minimize variance

across criteria and maximize alternative performance, enabling proactive risk management, and enhancing the overall resilience of energy infrastructure. To this end, the SECA approach begins by identifying the criteria that can play a decisive role in identifying the critical contingencies in integrated PDNs and DHNs. The selected criteria in this study are expected energy not supplied, maximum feeder loading margin, and renewable power curtailment rate against feeder failures. To enable objective evaluation, it is necessary to quantify each criterion. Therefore, the expected power and heat not supplied can be quantified in terms of the amount of electrical and thermal loads that can be shed in response to system disturbances, as stated in (1a) and (1b). The value of lost load, which takes into account the status of both critical and non-critical subscribers, along with operational and security grid codes, is a crucial factor in determining the impact of changes to the aforementioned criteria. Distribution system operators consistently endeavor to diminish the expected energy not supplied criterion, also known as the non-beneficial criterion (*NC*). The power feeder with the highest load shedding rate following an unexpected event occurs is inherently considered the most critical contingency scenario. Based on (1c), the maximum feeder loading margin, which is a security-oriented operational parameter, can be quantified as the percentage of occupied capacity in each feeder under different operational conditions. The loading margin indicates the changes in power flow across each feeder when unwanted tripping occurs at different power lines, i.e., $S^{AF}_{ij,t}$, relative to the normal conditions in the same feeder, i.e., $S^{BF}_{ij,t}$. An increase in the loading margin results in a feeder becoming more critical and more susceptible, which is why this criterion is regarded as a non-beneficial criterion, given that the operator's objective is to decrease it. Additionally, the renewable power curtailment criterion, which is an energy security criterion, can be quantified as the ratio of the dispatched renewable power, i.e., $P^{RES}_{i,t}$, to the available renewable power capacity, i.e., $\widetilde{P^{RES}_{i,t}}$, as shown in (1d). The renewable power curtailment rate is considered a non-beneficial criterion within the SECA approach because the high curtailment rate of RESs will result in integrated energy networks becoming more vulnerable to disruption during stressful situations. The implementation of this data-driven SECA approach necessitates the calculation of optimal values for each criterion individually, in the event of tripping in each feeder during peak load periods. To this end, the integrated energy networks must be optimally scheduled in a manner that minimizes both critical and non-critical load-shedding rates, in accordance with established security and operational constraints, following the tripping of each feeder. It is important to note that to prioritize critical PDN feeders, CHP units and ESSs are excluded from consideration. This is done to ensure that the most vulnerable structure possible for integrated energy networks is studied in determining critical contingency scenarios. Once the criteria have been quantified, the multi-criteria optimization problem, which can be found in our latest paper [18], must be solved to ascertain operational criterion weights and identify critical contingency scenarios. The optimization problem is designed to maximize the performance score of each of the alternatives by minimizing variance within and between the criteria in the context of the SECA method. A lower score indicates a heightened criticality scenario, while a higher score indicates a lower criticality scenario. In contrast to traditional N-k analysis, which enumerates component outages without differentiation, the SECA-based multi-criteria approach provides a ranking that reflects the relative severity of feeder contingencies in terms of service continuity, security margins, and renewable integration. This ensures that contingencies with the most significant cross-sectoral consequences are prioritized rather than treated equally. Furthermore, unlike probabilistic risk-based approaches that rely heavily on subjective or uncertain probability assignments, SECA employs a fully data-driven weighting of criteria, thereby enhancing transparency and minimizing bias. This integration of techno-economic, security, and sustainability criteria offers a more comprehensive basis for identifying critical contingencies in interdependent PDN–DHN systems.

$$\%\mathcal{EPNS} = \sum_{t\in\mathcal{T}}\sum_{i\in\mathcal{I}}\left[\frac{\left(1-\gamma^{P}_{i,t}\right)\left(\widehat{P^{D}_{i,t}}+\widetilde{P^{D}_{i,t}}\right)}{P^{D}_{i,t}}\right]\times 100; \tag{1a}$$

$$\%\mathcal{EHNS} = \sum_{t\in\mathcal{T}}\sum_{n\in\mathcal{N}}\left[\frac{\left(1-\gamma^{H}_{n,t}\right)\left(\widehat{H^{D}_{n,t}}+\widetilde{H^{D}_{n,t}}\right)}{H^{D}_{n,t}}\right]\times 100; \tag{1b}$$

$$\%\mathcal{LM} = max\left\{\left(\frac{\left|S^{AF}_{ij,t}\right|-\left|S^{BF}_{ij,t}\right|}{\left|S^{BF}_{ij,t}\right|}\right)\times 100, \forall t, ij\in\mathcal{L}\right\}; \tag{1c}$$

$$\%\mathcal{RPC} = \left(\frac{\widehat{P^{RES}_{i,t}}-P^{RES}_{i,t}}{\widehat{P^{RES}_{i,t}}}\right)\times 100, \quad \forall i,t. \tag{1d}$$

Let the critical contingency scenarios $s\in\mathcal{S}$ represent the failure of subset $\mathcal{L}_s=\{1,....,l_s\}$ of set of power feeders $\mathcal{L}$, where each contingency scenario $l_s\in\mathcal{L}_s$ is expressed by a triplet $\left(l,t^{f}_{s,l_s},t^{cl}_{s,l_s}\right)$. After identifying and prioritizing the critical feeders by employing the SECA approach, a subset of the most critical feeders $\mathcal{L}_s$ is selected to define critical N-1 and N-k contingency scenarios according to the conservatism level of distribution system operators, as well as whether the integrated energy network is strategic or not. t^{f}_{s,l_s} and t^{cl}_{s,l_s} indicating the fault occurrence time and fault clearing time in feeder l in scenario s. The restoration time is dependent on the duration it takes for the repair crew to restore the damaged feeder.

B. Failure analysis model for PDNs

The aim of the developed failure analysis model of PDNs is to minimize the expected cost of unserved electrical loads subsequent to the occurrence of critical contingency scenarios in power distribution feeders. To achieve this, a linear and convex optimization model for resiliency-oriented day-ahead scheduling of integrated PDNs and DHNs is developed to satisfy N-1 and N-K security under critical contingency modes. The decision-making problem to analyze the failure rate of PDNs during critical contingency events caused by unexpected events is manifested in (2a) and (2b).

$$\min_{\Xi_1}: \sum_{t\in\mathcal{T}}\sum_{i\in\mathcal{I}}\left(1-\gamma^{P}_{i,t,s}\right)\left(ENS^{pcr}_{i}\widehat{P^{D}_{i,t}}+ENS^{pncr}_{i}\widetilde{P^{D}_{i,t}}\right), \forall s\in\mathcal{S}; \tag{2a}$$

$$s.t. \qquad 0\le\gamma^{P}_{i,t,s}\le 1, \quad \forall i,t,s. \tag{2b}$$

1) PDNs operation constraints: The day-ahead resilient operation of PDNs is subject to a set of operational constraints, which hold for $\forall s\in\mathcal{S}$ and $\forall t\in\mathcal{T}$. Constraints (3a) and (3b) guarantee the nodal active and reactive power balance for each scenario s and each time slot t, respectively. The active and reactive power balance equations rely on a linearized AC power flow model for radial topology. This model incorporates the loss factor into the model and has been widely implemented in PDNs [19], [20] and integrated PDNs and DHNs [21]. The linearized model is presented in (3c)-(3g). The thermal limit of the feeder and voltage magnitudes should be within secure ranges, as specified in (3h) and (3i), to ensure soft operation constraints are met. Auxiliary binary parameter $\alpha_{l,t,s}$ in (3h) represents the status of feeder l at time t for contingency scenario s. In addition, (3j) sets the voltage magnitude and phase angle at the slack bus.

$$P^{grid}_{i,t,s}\Big|_{i=1} + P^{WT}_{i,t,s} + P^{PV}_{i,t,s} + \sum_{u\in\mathcal{U}_i} P^{CHP}_{u,t,s} + P^{ES,dis}_{i,t,s} - P^{ES,ch}_{i,t,s} - \gamma^{P}_{i,t,s} P^{D}_{i,t} - \sum_{g\in\mathcal{G}_i} P^{PtH}_{g,t,s} = P^{inj}_{i,t,s}, \forall i,t,s; \tag{3a}$$

$$Q^{grid}_{i,t,s}\Big|_{i=1} + Q^{WT}_{i,t,s} - \gamma^{P}_{i,t,s} Q^{D}_{i,t} = Q^{inj}_{i,t,s}, \qquad \forall i,t,s; \tag{3b}$$

$$\frac{P^{inj}_{i,t,s}}{Sb} = \sum_{\substack{j\in\mathcal{I}\\ j\neq i}} \Big(g^{y}_{ij}\left(v_{i,t,s}+v_{j,t,s}-1\right) + b^{y}_{ij}\left(\theta_{i,t,s}-\theta_{j,t,s}\right)\Big) + g^{y}_{ii}\left(2v_{i,t,s}-1\right), \quad \forall i,t,s; \tag{3c}$$

$$\frac{Q^{inj}_{i,t,s}}{Sb} = \sum_{\substack{j\in\mathcal{I}\\ j\neq i}} \Big(-b^{y}_{ij}\left(v_{i,t,s}+v_{j,t,s}-1\right) + g^{y}_{ij}\left(\theta_{i,t,s}-\theta_{j,t,s}\right)\Big) - b^{y}_{ii}\left(2v_{i,t,s}-1\right), \quad \forall i,t,s; \tag{3d}$$

$$P_{ij,t,s} = Sb\left[-g^{y}_{ij}\left(v_{i,t,s}-v_{j,t,s}\right) + b^{y}_{ij}\left(\theta_{i,t,s}-\theta_{j,t,s}\right)\right], \forall ij\in\mathcal{L}; \tag{3e}$$

$$Q_{ij,t,s} = Sb\left[b^{y}_{ij}\left(v_{i,t,s}-v_{j,t,s}\right) + g^{y}_{ij}\left(\theta_{i,t,s}-\theta_{j,t,s}\right)\right], \forall ij\in\mathcal{L}; \tag{3f}$$

$$S_{ij,t,s} = P_{ij,t,s} + \xi_{ij,t}\cdot Q_{ij,t,s}, \quad \forall t,s,ij\in\mathcal{L}; \tag{3g}$$

$$-\overline{S_l}\cdot\alpha_{l,t,s} \le S_{l,t,s} \le \overline{S_l}\cdot\alpha_{l,t,s}, \ \forall t,s,l\in\mathcal{L}; \tag{3h}$$

$$\underline{v_i} \le v_{i,t,s} \le \overline{v_i}, \ \ \forall i,t,s; \tag{3i}$$

$$\theta_{i,t,s} = 0, \quad v_{i,t,s} = 1, \ \ \forall i = 1,t,s. \tag{3j}$$

2) Models of RESs and BESSs: The active and reactive power supplied by wind turbines are restricted by (4a) and (4b), while the actual active power produced by PV systems is constrained by (4c). The active power charge and discharge of BESSs in each period are bounded to their maximum capacity $\overline{P^{ES}_i}$ as specified in (4d) to describe the operational and technical limits of BESSs. The use of the tractable exact approximation in (4e) prevents the simultaneous charging and discharging of BESSs in each time slot. This constraint eliminates the need for binary variables in the modeling of BESSs. Empirical observations confirm the correctness of this approximation in the conducted simulations. The state constraint for BESSs is formulated in (4f). Inequality (4g) guarantees that the state-of-charge of BESSs is restricted to the minimum required storage, i.e., $\underline{SoC^{ES}_i}$, and the maximum storage capacity, i.e., $\overline{SoC^{ES}_i}$. Furthermore, (4h) ensures that the state-of-charge of BESSs remains the same in the first and last time slots of the resiliency-oriented day-ahead scheduling problem.

$$0 \le P^{WT}_{i,t,s}\Delta t \le \widehat{P^{WT}_{i,t}}, \quad \forall i,t,s; \tag{4a}$$

$$-PF_i^{WT}\widehat{P^{WT}_{i,t}} \le Q^{WT}_{i,t,s} \le PF_i^{WT}\widehat{P^{WT}_{i,t}}, \quad \forall i,t,s; \tag{4b}$$

$$0 \le P^{PV}_{i,t,s}\Delta t \le \widehat{P^{PV}_{i,t}}, \quad \forall i,t,s; \tag{4c}$$

$$0 \le P^{ES,dis}_{i,t,s}, \quad P^{ES,ch}_{i,t,s} \le \overline{P^{ES}_i}, \quad \forall i,t,s; \tag{4d}$$

$$\frac{P^{ES,ch}_{i,t,s}}{\overline{P^{ES}_i}} + \frac{P^{ES,dis}_{i,t,s}}{\overline{P^{ES}_i}} \le 1, \quad \forall i,t,s; \tag{4e}$$

$$SoC^{ES}_{i,t,s} = SoC^{ES,ini}_{i,s}\Big|_{t=1} + SoC^{ES}_{i,t-1,s}\Big|_{t>1} + \left(\eta^{ch}_i P^{ES,ch}_{i,t,s} - \frac{P^{ES,dis}_{i,t,s}}{\eta^{dis}_i}\right) \tag{4f}$$

$$\underline{SoC^{ES}_i} \le SoC^{ES}_{i,t,s} \le \overline{SoC^{ES}_i}, \quad \forall i,t,s; \tag{4g}$$

$$SoC^{ES,ini}_{i,s} = SoC^{ES}_{i,t,s}, \quad \forall t = \mathcal{T}, i, s. \tag{4h}$$

C. Cascading failure analysis model for heat shortage

The linear resilience optimization model is developed to analyze cascading heat shortages in DHNs following critical contingency scenarios in the power feeders. The proposed failure analysis model aims to minimize the duration of energy shortage and the cost associated with the ratio of unmet heat demand, i.e., $(1-\gamma^{H}_{n,t,s})$, in each node caused by critical N-1 or N-k contingencies on power feeders, as outlined in (5a) and (5b). The model ensures the continuity of mass flow in pipelines, taking into account factors such as geographic location and the criticality of affected nodes. It leverages the principles from multi-criteria decisions to inform the operational status of PtH units in various contingency scenarios to determine the optimal set-points of local backup resources to reach the resilient dispatch strategy of DHNs. It achieves this by intelligently deploying the stored energy in gas line pack and TESSs, as well as implementing the integrated DRP to reduce the impact of critical feeder outage contingencies on the heat supply, maintain heat balance, and optimize temperatures and flow rates along DHNs by controlling the amount of energy supplied to certain demands.

$$\min_{\Xi_2}: \sum_{t\in\mathcal{T}}\sum_{n\in\mathcal{N}} \left(1-\gamma^{H}_{n,t,s}\right)\left(ENS^{hcr}_{n}\widehat{H^{D}_{n,t}} + ENS^{hncr}_{n}\widehat{H^{D}_{n,t}}\right), \forall s\in\mathcal{S}; \tag{5a}$$

$$s.t. \qquad 0 \le \gamma^{H}_{n,t,s} \le 1, \quad \forall n,t,s. \tag{5b}$$

1) Pipeline model and continuity of mass flow in DHNs: To model DHNs under the CF-VT control strategy, constant mass flow rates and hydraulic conditions are assumed, while the circulating water temperatures are considered variable. The linear nodal method [22] can be used to model the operating limits of DHNs as well as the continuity of mass flow, taking into account both hydraulic and thermal conditions. The pipeline's thermal dynamic process and the relationship between the fluid's inlet and outlet temperatures along the supply and return pipelines are expressed by (6a)-(6c). Based on the principles of fluid dynamics, all inflows to a node with varying temperatures in the supply or return side of DHNs are combined, and the temperature of the mixed mass at confluence nodes, i.e., $\tau s^{mix}_{n,t,s}$ and $\tau r^{mix}_{n,t,s}$, can be calculated using (6d) and (6e) in accordance with the energy conservation law. The heat stations in DHNs are equipped with CHP units, PtH units, and TESSs as heat sources. The thermal energy supplied by heat stations is provided as (6f) and (6g). Constraint (6h) defines the relationship between heat power and supply and return temperatures. To ensure load-serving quality, it is necessary to maintain the supply and return temperatures of the heat station and exchanger nodes within a specified range, as indicated in (6i) and (6j). The heat balance for each node of district heating networks is derived based on the energy conservation law, as well as the mass flow rate, temperature, and heat transfer capacity of pipelines, as implied by (6k).

$$\tau s^{ou}_{p,t,s} = \left(\tau s^{in}_{p,t,s} - T^{am}_{p,t}\right) e^{-\frac{\lambda_p \kappa_p}{\rho \dot{m}_p}} + T^{am}_{p,t}, \quad \forall p,t,s; \tag{6a}$$

$$\tau r^{ou}_{p,t,s} = \left(\tau r^{in}_{p,t,s} - T^{am}_{p,t}\right) e^{-\frac{\lambda_p \kappa_p}{\rho \dot{m}_p}} + T^{am}_{p,t}, \quad \forall p,t,s; \tag{6b}$$

$$\underline{\tau} \le \tau s^{(\cdot)}_{p,t,s}, \quad \tau r^{(\cdot)}_{p,t,s} \le \overline{\tau}, \quad \forall p,t,s; \tag{6c}$$

$$\sum_{p\in\Lambda^{P-}_n}\left(\tau s^{ou}_{p,t,s}\dot{m}_p\right) + \sum_{o\in\Lambda^{\mathcal{Z}}_n}\left(\tau s^{Z}_{o,t,s}\dot{m}^{Z}_o\right) = \tau s^{mix}_{n,t,s}\left(\sum_{p\in\Lambda^{P-}_n}\dot{m}_p + \sum_{o\in\Lambda^{\mathcal{Z}}_n}\dot{m}^{Z}_o\right), \ \forall n,t,s; \tag{6d}$$

$$\sum_{p\in\Lambda^{P-}_n}\left(\tau r^{ou}_{p,t,s}\dot{m}_p\right) + \sum_{o\in\Lambda^{\mathcal{D}}_n}\left(\tau r^{D}_{o,t,s}\dot{m}^{D}_o\right) = \tau r^{mix}_{n,t,s}\left(\sum_{p\in\Lambda^{P-}_n}\dot{m}_p + \sum_{o\in\Lambda^{\mathcal{D}}_n}\dot{m}^{D}_o\right), \ \forall n,t,s; \tag{6e}$$

$$H^{Z}_{n,t,s} = \rho\dot{m}^{Z}_n\left(\tau s^{Z}_{n,t,s} - \tau r^{Z}_{n,t,s}\right), \quad \forall n,t,s; \tag{6f}$$

$$H^{Z}_{n,t,s} = \sum_{u\in\mathcal{U}_n} H^{CHP}_{u,t,s} + \sum_{g\in\mathcal{G}_n} H^{PtH}_{g,t,s} + H^{TS,dis}_{n,t,s} - H^{TS,ch}_{n,t,s}, \forall n,t,s; \tag{6g}$$

$$\gamma^{H}_{n,t,s}H^{D}_{n,t} = \rho\dot{m}^{D}_n\left(\tau s^{D}_{n,t,s} - \tau r^{D}_{n,t,s}\right), \quad \forall n,t,s; \tag{6h}$$

$$\underline{\tau s^{Z}_n} \le \tau s^{Z}_{n,t,s} \le \overline{\tau s^{Z}_n}, \qquad \underline{\tau s^{D}_n} \le \tau s^{D}_{n,t,s} \le \overline{\tau s^{D}_n}, \forall n,t,s; \tag{6i}$$

$$\underline{\tau r^{Z}_n} \le \tau r^{Z}_{n,t,s} \le \overline{\tau r^{Z}_n}, \qquad \underline{\tau r^{D}_n} \le \tau r^{D}_{n,t,s} \le \overline{\tau r^{D}_n}, \forall n,t,s; \tag{6j}$$

$$H^{Z}_{n,t,s} + \sum_{p\in\Lambda^{P-}_n}\rho\dot{m}_p\left(\tau s^{ou}_{p,t,s} + \tau r^{ou}_{p,t,s}\right) = \gamma^{H}_{n,t,s}H^{D}_{n,t} + \sum_{p\in\Lambda^{P+}_n}\rho\dot{m}_p\left(\tau s^{in}_{p,t,s} + \tau r^{in}_{p,t,s}\right), \quad \forall n,t,s. \tag{6k}$$

2) Models of PtH, CHP, and TESSs: Constraint (7a) indicates the relationship between the power consumption of PtH unit g and its heat generation. The power absorbed by the PtH units is limited by technical specifications (7b). The feasible operating region of CHP units is determined by the convex combination of the corner points, as specified by the set of constraints (7c)-(7e). The electric and heat power

output of the corner points are represented by $\widehat{P}_{u,f}^{CHP}$ and $\widehat{H}_{u,f}^{CHP}$. Since the dynamic modeling of TESSs and BESSs has the same form, the models associated with the TESSs were left out.

$$COP_g = -a\left[\frac{H_{g,t,s}^{PtH}}{P_{g,t,s}^{PtH}}\right] + b, \quad \forall g,t,s; \tag{7a}$$

$$0 \le P_{g,t,s}^{PtH} \le \overline{P_g^{PtH}}, \quad \forall g,t,s; \tag{7b}$$

$$P_{u,t,s}^{CHP} = \sum_{f\in\mathcal{F}} \beta_{f,u,t,s}\widehat{P}_{u,f}^{CHP}, H_{u,t,s}^{CHP} = \sum_{f\in\mathcal{F}} \beta_{f,u,t,s}\widehat{H}_{u,f}^{CHP}; \tag{7c}$$

$$\sum_{f\in\mathcal{F}} \beta_{f,u,t,s} = 1, \quad \forall u,t,s; \tag{7d}$$

$$0 \le \beta_{f,u,t,s} \le 1, \quad \forall f,u,t,s. \tag{7e}$$

D. Harvesting the demand-side response capacity to enhance integrated energy network resilience

Consumers can be categorized into two types of critical, i.e., $\widehat{P_{i,t}^D}$ and $\widehat{H_{i,t}^D}$, and controllable, i.e., $\widetilde{P_{i,t}^D}$ and $\widetilde{H_{i,t}^D}$, loads in integrated PDNs and DHNs, as stated in (8a) and (8b). Under the developed cascading failure analysis model for integrated PDNs and DHNs, the direct load control approach allows operators to shed a portion of the non-essential or controllable loads from the avoidance stage to the post-disaster stage in the response to N-1 or N-k contingencies on power feeders. This strategy reduces strain on the integrated energy networks, prevents overloads, and ensures essential services for critical consumers remain operational. Constraints (8c) and (8d) impose a ceiling on the maximum allowable energy reduction for controllable consumers during each contingency scenario, contingent on the participation rates of these consumers, i.e, ϕ^P and ϕ^H, in the direct load control program. By combining the integrated DRPs with the developed cascading failure model, term "$\gamma_{i,t,s}^P P_{i,t}^D - \Delta P_{i,t,s}^{IDR}$" should replace term "$\gamma_{i,t,s}^P P_{i,t}^D$" in (3a), term "$\gamma_{i,t,s}^P Q_{i,t}^D - PF_i^D \Delta P_{i,t,s}^{IDR}$" should replace term "$\gamma_{i,t,s}^P Q_{i,t}^D$" in (3b), and term "$\gamma_{n,t,s}^H H_{n,t}^D - \Delta H_{n,t,s}^{IDR}$" should replace term "$\gamma_{n,t,s}^H H_{n,t}^D$" in (6h) and (6k) to consider the impacts of controllable consumers on the resilient behavior of the integrated PDNs and DHNs.

$$P_{i,t}^D = \widehat{P_{i,t}^D} + \widetilde{P_{i,t}^D}, \quad \forall i,t; \tag{8a}$$

$$H_{n,t}^D = \widehat{H_{i,t}^D} + \widetilde{H_{i,t}^D}, \quad \forall n,t; \tag{8b}$$

$$0 \le \Delta P_{i,t,s}^{IDR} \le \phi^P \cdot \widetilde{P_{i,t}^D}, \quad \forall i,t,s; \tag{8c}$$

$$0 \le \Delta H_{n,t,s}^{IDR} \le \phi^H \cdot \widetilde{H_{i,t}^D}, \quad \forall n,t,s. \tag{8d}$$

III. Resilience KPIs for Integrated PDNs and DHNs

By optimizing the ratios of power and heat served, i.e., $\gamma_{i,t,s}^P$ and $\gamma_{n,t,s}^H$, through the implementation of failure analysis models for a set of contingency scenarios $\mathcal{S}$ during $\mathcal{T}$, the interdependence between the resilience of PDNs and DHNs can be quantified. To define resilience KPIs, we first define two practical metrics, namely power serving capability, i.e., $\mathcal{PSC}(t)$, and heat serving capability, i.e., $\mathcal{HSC}(t)$, as (9a) and (9b). These metrics reflect the average ratio of power and heat served, respectively, by the PDN and DHN for all defined contingency scenarios during $\mathcal{T}$. Based on the different phases of the contingency chain, Fig. 3 hypothetically shows the impact of critical contingencies on power feeders on the evolution of $\mathcal{PSC}(t)$ metric and the cascading failure of DHNs, denoted by $\mathcal{HSC}(t)$, taking into account resilience attributes. As illustrated in Fig. 3, the contingency chain extends from the pre-contingency to the post-contingency phases. Prior to the pre-contingency phase, which spans from $t=0$ until $t=t_{ds}^P$, the integrated PDNs and DHNs operate under normal conditions. At the time $t=t_{ds}^P$, one of the critical N-1 or N-k contingency scenarios on power feeders may occur, potentially damaging several power feeders over a certain period. As none of the pipelines fail, unlike the PDN, where CHP units may fail to support parts of the grid, heat loads will be supplied until

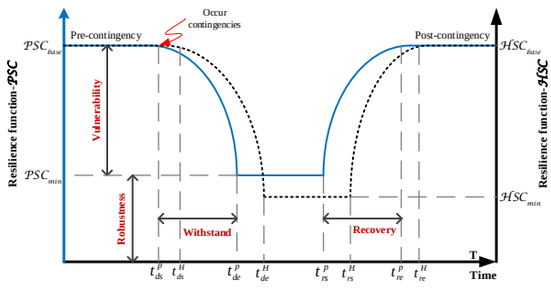

Fig. 3. Assessment of the chronological contingency of power and heat serving capability.

the line pack storage capacity is not exhausted. Therefore, the impact of the power outage on DHNs, in terms of heat shortage, will begin slightly later. After the start of the critical contingencies, i.e., from $t=t_{ds}^P$ to $t=t_{de}^P$, the serving capability of the PDN faces a severe drop compared to the initial conditions $\mathcal{PSC}_{base}$, in which the serving capability metric decreases to $\mathcal{PSC}_{min}$. The operator can withstand load shedding to the extent that backup resources embedded in the PDNs, i.e., the capacity of BESSs, line pack, CHP units, RESs, and controllable loads, allow. The optimal operation of the DHNs can degrade, i.e., $\mathcal{HSC}_{min}$, at a different time $t=t_{de}^H$ than the PDN due to various factors. These factors include the capacity of TESSs, the location of out-of-service PtH units, the line pack capacity, and the participation of thermal loads in integrated DRPs. After the contingencies caused by external disturbances subside at $t=t_{rs}^P$, the repair crew takes action to restore the PDN until $t=t_{re}^P$, at which point the PDN returns to its normal condition, i.e., post-contingency condition. The PtH units' restoration starts after the damaged feeders' recovery at time $t=t_{rs}^P$, and the scheduled heat power by these units is injected into the pipelines again at $t=t_{re}^H$. It is important to note that after time slot $t=t_{rs}^P$, once the unexpected contingencies have been cleared, the gas network infrastructure will continue to operate normally. The interdependence between the resilience of PDNs and DHNs can be assessed using the following resilience KPIs.

1) *Relative impact of PDN disturbances on the resilient operation of DHN ($\mathcal{DR}$):* The KPI emphasizes the dependency of DHNs on the stability of the PDNs during critical contingencies, as stated in (9c).
2) *DHN sensitivity to PDN degradation ($\mathcal{SD}$):* This KPI evaluates the correlation between PDN and DHN performances during the failure phase. The KPI provides insight into how quickly and severely the DHN is affected by PDN degradation. It can be measured using (9d).
3) *DHN recovery dependence to PDN restoration ($\mathcal{RR}$):* This KPI indicates the degree to which the recovery rapidity of the DHN is linked to the duration of the transition of the PDN from the degraded phase to the post-contingency phase, as expressed in (9e).

$$\mathcal{PSC}(t) = \frac{1}{\mathcal{I}\cdot\mathcal{S}}\sum_{i\in\mathcal{I}}\sum_{s\in\mathcal{S}}\gamma_{i,t,s}^P, \quad \forall t; \tag{9a}$$

$$\mathcal{HSC}(t) = \frac{1}{\mathcal{N}\cdot\mathcal{S}}\sum_{n\in\mathcal{N}}\sum_{s\in\mathcal{S}}\gamma_{n,t,s}^H, \quad \forall t; \tag{9b}$$

$$\mathcal{DR} = \sum_{t\in\mathcal{T}}\frac{\mathcal{HSC}(t)}{\mathcal{PSC}(t)}; \tag{9c}$$

$$\mathcal{SD} = \frac{\mathcal{HSC}_{base}-\mathcal{HSC}_{min}}{\mathcal{PSC}_{base}-\mathcal{PSC}_{min}} \times \frac{t_{ds}^P - t_{de}^P}{t_{ds}^H - t_{de}^H}; \tag{9d}$$

$$\mathcal{RR} = \frac{\mathcal{HSC}_{base}-\mathcal{HSC}_{min}}{\mathcal{PSC}_{base}-\mathcal{PSC}_{min}} \times \frac{t_{re}^P - t_{rs}^P}{t_{re}^H - t_{rs}^H}. \tag{9e}$$

In contrast to conventional resilience KPIs, such as the resilience triangle, time-to-recovery, or load loss ratio, which are either scalar or single-domain, the proposed indices are normalized, interpretable, and inter-layer sensitive. Consequently, they are well-suited for matrix-based evaluation frameworks such as SECA. The utilization of SECA as

the primary ranking method demands meticulously designed KPIs that maintain system-specific interdependencies and facilitate equitable concurrent evaluation of critical scenarios. The proposed resilience indices have been meticulously crafted to fulfill this function. These KPIs necessitate only static system data and scenario-based contingency inputs, rendering them highly suitable for planning applications that do not rely on dynamic time-domain simulations.

IV. Numerical Simulations

A. System configurations and case studies description

In this section, the IEEE 33-bus PDN and a 32-node DHN are employed to assess the resilience of heat-power integrated energy systems using a multi-criteria decision-making failure analysis model developed for this purpose. The standard test system is modified to consider a futuristic version of an integrated energy system with a high penetration of sustainable green energy generation and conversion sources. The topology of the modified interdependent PDN and DHN test system is depicted in Fig. 4. The data for DHN data can be found in [23]. To satisfy the reactive power balance constraint in some N-k contingency scenarios, a 70 kVAR capacitor has been installed in bus 8 of the PDN. The power and heat demand profiles are illustrated in Fig. 5(a), with peak demand values of PDN and DHN at 4.65 MW+j 2.79 MVAR and 3.45 MW, respectively. It should be noted that 30% of demand at each PDN's bus and DHN's node is allocated to critical loads. The percentage of the maximum daily amount of the forecasted output power of wind turbines and PV systems, along with the ambient temperature, are provided in Fig. 5(b). Each CHP unit has a capacity of 0.8 MW. All PtH units have a nominal capacity of 1 MW and a coefficient of performance of 2. The TESSs and BESSs are operated in the integrated energy system with a maximum charging and discharging power and heat of 1 MW and 0.5 MW, respectively. A set of wind-based and PV-based non-dispatchable renewable distributed generators are allocated at buses 5, 19, 32, and 15 with a rated power of 1 MW, 1 MW, 0.5 MW, and 0.5 MW, respectively. The load shedding penalty cost for electrical demands of critical and non-critical importance, in addition to those for heat demands of a similar nature, are scheduled to amount to 6000 \$/MWh, 2000 \$/MWh, 3000 \$/MWh, and 1000 \$/MWh, respectively [24]. Additionally, it is presumed that the integrated DRP is accessible to the distribution system operator as a backup resilience tool, involving 10% of non-critical electricity subscribers and 5% of thermal subscribers in participation.

The final optimization model proposed in this paper is a convex Mixed-Integer Linear Programming (MILP) formulation. The nonlinearities inherent in the developed contingency multi-criteria assessment framework have been meticulously linearized through the implementation of enhanced approximation techniques, as elucidated in Section II. The formulated MILP model is solved by employing the CPLEX solver within the GAMS framework. Due to the convex nature of the model and the utilization of a globally optimal solver, the convergence to the global optimum is mathematically guaranteed. In all case studies, the optimality gap was found to be zero, thereby ensuring the convergence and reliability of the obtained solutions.

B. Results and technical discussions

Prior to implementing the cascade failure model and evaluating the resilience level of the test system, it is first necessary to prioritize the PDN feeders to identify the critical points within the integrated energy system. For this purpose, the decision matrix, as a data set of 32 power feeders, is constructed which incorporates the quantified performance values of each criterion related to the tripping of each power feeder during the peak power

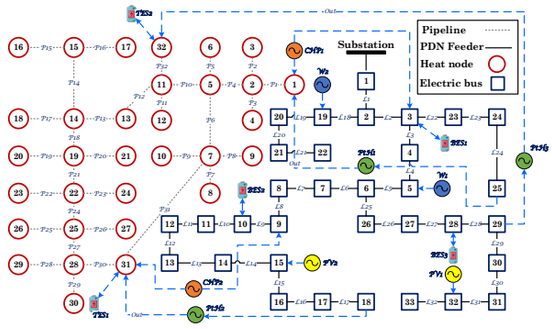

Fig. 4. Schematic diagram of the integrated test 33-bus PDN and 32-node DHN.

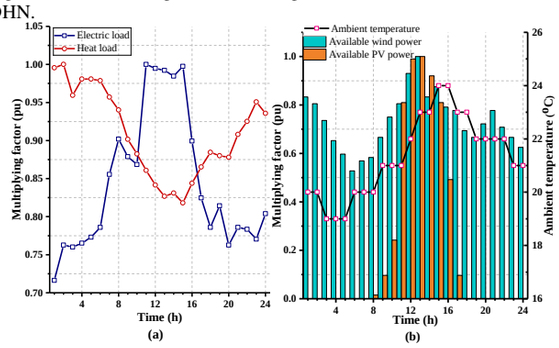

Fig. 5. The estimated value of (a) electrical and heating load profiles; and (b) renewable power generation and ambient temperature during the scheduling horizon.

TABLE II
Normalized Standard Deviation and Correlation of Criteria Resulting from Weighted Decision Matrix

Reference points	$\%\mathcal{EPNS}$	$\%\mathcal{EHNS}$	$\%\mathcal{LM}$	$\%\mathcal{RPC}$
$\widetilde{\sigma_y}$	0.0782	0.0941	0.3059	0.5216
$\widetilde{\pi_y}$	-0.0061	0.3237	0.3921	0.2902

period, i.e. $t = 11$. All four criteria are deemed to be non-beneficial criteria, which is reflected in the inverse relationship between the weighted values of the criteria and resilience performance. Consequently, the most critical feeders are those with the highest weighted values for $\mathcal{EPNS}$, $\mathcal{EHNS}$, $\mathcal{LM}$, and $\mathcal{RPC}$ criteria. To ascertain the conflict between each criterion and its counterpart criteria for each feeder, as well as to assess the alterations to a criterion across all existing feeders, correlation and standard deviation parameters serve as reference points for the SCEA method. The normalized results of these reference points for each criterion are reported in Table II. The higher standard deviation and correlation values for each criterion serve to reinforce the importance of that criterion over other criteria for the identification of system critical points. The performance scores of the alternatives are determined by optimizing the SECA multi-criteria decision-making problem, with the value of ζ set to 3, to rank the power feeders and identify the list of critical feeders. The results of the prioritization of critical feeders are presented in Table III. This table reveals that feeders $l5$ and $l6$ exhibit the greatest degree of criticality, as evidenced by their elevated $\mathcal{EPNS}$, $\mathcal{EHNS}$, $\mathcal{LM}$, and almost $\mathcal{RPC}$ indicators. These indicators are indicative of poor performance, as evidenced by their lowest performance scores among other feeders. Conversely, feeder $l17$ has the most favorable qualification within the test system, having scored 0.5818. The initial objective of the study is to develop a criticality-based assessment framework that supports risk-aware decision-making in integrated PDN-DHN systems, a goal that is accomplished by prioritizing feeders.

To fulfill the second and third objectives, which entail the modeling of cascading outages under severe contingencies as well as the evaluation of resilience enhancement tools, simulations are conducted on the basis of the most critical feeder outages. The ten most critical outage states that exhibited the greatest potential for failure within the test system, i.e., rank order 1-10 as presented in Table III, are

TABLE III
PRIORITIZING OF PDN FEEDERS BASED ON CRITICALITY

Rank no.	PDN feeder no.	S_l	Rank no.	PDN feeder no.	S_l
1	$l5$	0.2264	17	$l30$	0.3041
2	$l6$	0.2282	18	$l19$	0.3042
3	$l1$	0.2358	19	$l31$	0.3051
4	$l7$	0.2385	20	$l20$	0.3053
5	$l8$	0.2519	21	$l32$	0.3059
6	$l2$	0.2541	22	$l21$	0.3062
7	$l22$	0.2717	23	$l18$	0.3072
8	$l23$	0.2727	24	$l9$	0.3096
9	$l24$	0.2737	25	$l10$	0.3105
10	$l3$	0.2909	26	$l11$	0.3113
11	$l4$	0.2916	27	$l12$	0.3122
12	$l25$	0.2994	28	$l13$	0.3131
13	$l26$	0.3002	29	$l14$	0.314
14	$l27$	0.3011	30	$l15$	0.5798
15	$l28$	0.302	31	$l16$	0.5808
16	$l29$	0.3032	32	$l17$	0.5818

TABLE IV
NUMERICAL CASE STUDIES SPECIFICATIONS

Case no.	Type of contingency scenario	Deployed energy generation/conversion sources	Line pack storage capacity	Backup sources
Case 1	N-1 mode	CHP, PtH, RESs	Not considered	-
Case 2	N-k mode			-
Case 3	N-1 mode	CHP, PtH, RESs	Considered	-
Case 4	N-k mode			-
Case 5	N-k mode			ESSs
Case 6	N-k mode			ESSs & integrated DRP

considered in terms of their resilience to N-1 and N-k contingency scenarios to implement the developed cascading failure analysis model. The set of contingencies encompasses both single-line and multiple-line outages, which may divide the integrated energy system into distinct islands. The normal probability distribution function is employed to assess the likelihood of these events occurring at a specific time. To elicit the most unfavorable situation, the mean value of the function is assumed to be 11:00, which represents the peak electrical load time interval. The standard deviation, representing the dispersion of the probability distribution function, is set at two hours. The dispatch times of crew teams to perform repairs and restore damaged PDN feeders are also sampled from a normal distribution. The mean value is equal to six hours, which has been the average repair time sampled by distribution companies. The standard deviation is considered to be one hour, which is applied to all feeders. In consideration of the aforementioned statistical framework for changes in the normal distribution function, 20 randomly selected scenarios for the occurrence time of failures and the time it takes to clear the fault are drawn for each of the representative N-1 and N-k contingency events. The expected value obtained for each resilience metric is then reported in the results. In accordance with the delineated critical N-1 and N-k contingency scenarios, six cases are subjected to a comprehensive examination to recognize the resilience KPIs of the test system in the event of a cascading failure. These cases are outlined in Table IV. These cases encompass a diverse range of realistic upgrades to the integrated PDNs and DHNs, including the incorporation of RESs, PtH units, and CHP units at various locations, in addition to an increase in the line pack storage capacity of pipelines.

Table V presents the detailed results of the resilience KPIs of interdependent PDNs and DHNs for all cases. The results obtained in Cases 1 and 2 indicate that the performance of the DHN deteriorates rapidly when defined N-1 and N-k contingencies occur at PDN feeders during the damage periods. In these cases, the value of $\mathcal{DR}$ KPI is equal to 0.9418 and 0.8908, respectively. These values represent the lowest observed values among all cases, indicating the profound impact of PDN disturbances on the PtH units that supply an appreciable portion of the energy requirements of the DHN. In Case 2, the value of $\mathcal{SD}$ KPI, which represents the DHN's sensitivity to the PDN's degradation, is equal to 1.3439, which is the highest value observed in the remaining cases. This value is lower in Case 1 due to the lower outage severity. This discrepancy can be attributed to the absence of consideration for backup resilience tools in these cases, which has led to a significant increase in the vulnerability of the integrated energy system during the occurrence of cascading failures under critical contingencies. In Cases 3 and 4, where the line pack storage capacity permits the continued operation of CHP units for a limited period following the onset of PDN feeder outages, the DHN was successful in servicing the critical loads for a longer period following the power failure in the PtH units. Furthermore, the activation of the line pack storage capacity in Cases 3 and 4 has resulted in a reduction in the cascading decay rate in comparison to Cases 1 and 2. This is evidenced by the 5.765% and 8.185% reductions in the $\mathcal{SD}$ KPI, as presented in Table V. The temporal evolution of power and heat serving capability metrics in Cases 1, 3, and 4 is presented in Fig. 6 for the purpose of conducting a detailed microscopic analysis of the impacts of outage severity and the line pack storage capacity. Fig. 6 depicts the phenomenon of declining serviceability of both heat and power at hour 9:00. This is accompanied by a deterioration of the DHN. This phenomenon continues until time 10:30 in Case 3 and 9:45 in Case 4. The recovery process after clearing these contingencies does resemble Cases 1 and 2 to a considerable extent, indicating that this hypothesis may not be entirely valid. In Case 4 the power serviceability of PDN declines to 0.5679 at hour 16:00, as a result of the heightened disturbance caused by multiple outage scenarios. This is below the minimum value of the $\mathcal{PSC}$ metric in Case 3. This issue indicates a significant reduction in the robustness of the integrated energy system in response to N-k contingencies. In Case 3 versus Case 4, the critical and non-critical heat demand is supplied for a period of two hours following the occurrence of power outages. Thereafter, the DHN attempts to maintain the critical loads alive in the withstand phase for a period of 4:30 hours, before reaching the minimum heat serving capacity of 0.5751. Moreover, as concluded from Fig. 6, the implementation of single-outage scenarios in Case 3 has resulted in a 2-hour reduction in the time required for the repair and recovery process, with the interdependent PDN and DHN entering the post-contingency phase at 19:00.

The capacity of the integrated energy system to supply power and heat, as demonstrated in Cases 5 and 6, in which BESSs and TESSs are integrated into the test system and the integrated DRP is made available to the distribution system operator as a supplementary resilience measure, is illustrated and contrasted with the findings in Case 4, as shown in Fig. 7. As demonstrated results in Fig. 7, deployment of the BESSs and TESSs resulted in a 5.26% and 8.79% increase in the supplied electrical and thermal loads, respectively, compared to the same contingency mode in Case 4. This is due to the fact that, by simulating different contingency scenarios, the ESSs have been operated in coordination with the line pack storage capacity during the damage period, specifically between 13:00 and 19:00, with the maximum possible capacity in the discharge mode. In Case 5, the sensitivity of the DHN to the PDN feeders degradation, as indicated by the $\mathcal{SD}$ KPI, is reduced by 14.247% compared to Case 4. This is because BESS 3 is located near one of the heat stations, i.e., PtH unit 3, and TESSs are embedded in nodes 31 and 32. As illustrated in Table V and Fig. 7, the superiority of Case 6 is evident, as the implementation of the integrated DRP allows the distribution system operator to employ line pack storage capacity in optimal coordination with BESSs and TESSs in a rational manner, thereby enhancing the robustness of the integrated energy system by 32.92% in comparison to Case 5. In Case 6, the $\mathcal{SD}$ KPI exhibited a 10% decrease and the $\mathcal{DR}$ KPI displayed a 20% surge in comparison to the obtained results from Case 5, as backup resources reduce the degradation rate of heat supply. This outcome indicates that the sensitivity to PDN degradation and the reliance on PDN restoration have undergone a significant decline in comparison to Case 5. From this, it can thus be concluded that DHN is ca-

TABLE V
RESILIENCE KPIS COMPARISON FOR CASE STUDIES

Case no.	$\mathcal{DR}$	$\mathcal{SD}$	$\mathcal{RR}$
Case 1	0.9418	1.2402	1.1801
Case 2	0.8908	1.3439	1.3206
Case 3	0.9719	1.1687	1.1801
Case 4	0.9458	1.2339	1.3186
Case 5	0.9807	1.0581	0.8408
Case 6	1.0268	0.9662	0.7938

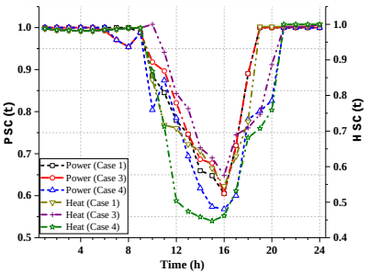

Fig. 6. Comparison of power and heat serving capability metrics in Cases 1, 3, and 4.

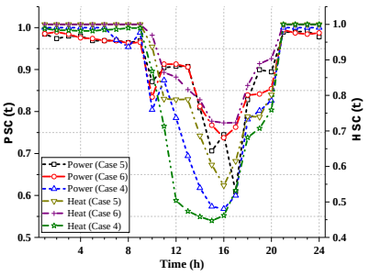

Fig. 7. Comparison of power and heat serving capability metrics in Cases 4, 5, and 6.

pable of operating in conjunction with the existing local power generation facilities while simultaneously managing the consumption levels of non-critical subscribers. This has resulted in the achievement of a reliable DHN that is capable of providing a significant extent, approximately 92.17%, of the customer's thermal demands, even in the presence of critical N-k contingencies. The integration of the integrated DRP with BESSs also enhances the operational effectiveness of the PDN. As demonstrated by the PSC curve for Case 6 in Fig. 7, the PDN experiences a mere 9.089% non-critical load curtailment across all N-k contingency scenarios. This is due to the fact that the energy supply is constrained to the envisaged contingency chain, in addition to the compromise made between critical users in the PDN and DHN.

1) Impact of the penetration rate of backup tools on resilience performance of test system: To illustrate the benefits of backup tools in the interdependence between the resilience of the PDNs and DHNs, the influences of different scales of the BESSs and TESSs as well as the participation rate of controllable consumers in the integrated DRP on the aforementioned resilience KPIs are investigated. To this end, the out-of-sample simulation is implemented with the intention of re-evaluating the developed cascading failure analysis model, taking into account the varying degrees of backup resilience tools. To calculate the resilience KPIs, 50, 80, and 100 out-of-sample outage scenarios are drawn based on the configuration of Case 6. It should be noted that the various N-k outage scenarios are applied sequentially to samples (S_n) drawn from a set consisting of 12 elements, as follows: $S_1 : (0.6, 10\%, 5\%), S_2 : (0.6, 15\%, 10\%), S_3 : (0.6, 20\%, 15\%), S_4 : (1, 10\%, 5\%), S_5 : (1, 15\%, 10\%), S_6 : (1, 20\%, 15\%), S_7 : (1.2, 10\%, 5\%), S_8 : (1.2, 15\%, 10\%), S_9 : (1.2, 20\%, 15\%), S_{10} : (1.8, 10\%, 5\%), S_{11} : (1.8, 15\%, 10\%), S_{12} : (1.8, 20\%, 15\%)$. In this set, the first element represents the capacity of ESSs relative to the initial value, while the second and third elements represent the participation rates of controllable electrical and heat consumers in the integrated DRP, respectively.

TABLE VI
RESILIENCE KPIS COMPARISON BASED ON DIFFERENT OUT-OF-SAMPLE SCENARIOS IN CASE 6

Sample no. in Case 6	No. of scenarios	Expected values		
		$\mathcal{DR}$	$\mathcal{SD}$	$\mathcal{RR}$
S_1	80	0.9763	1.0748	0.8342
S_3		0.9865	1.0665	0.8231
S_4	50	1.0268	0.9662	0.7938
S_6		1.0368	0.9591	0.7529
S_{10}	100	1.0593	0.5494	0.6771
S_{12}		1.0744	0.5006	0.5191

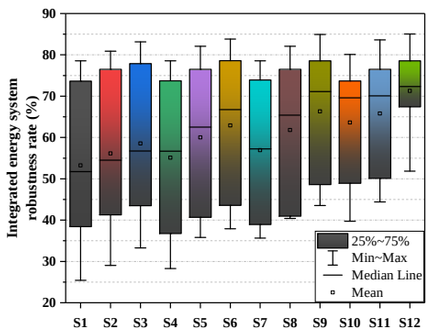

Fig. 8. Robustness degree of the integrated energy system in response to variations in penetration levels of backup sources for Case 6.

The expected value obtained for each resilience KPI for some important samples is presented in Table VI. The results indicate that the value of $\mathcal{SD}$ and $\mathcal{RR}$ KPIs varies by 48.88% and 18.83%, respectively, when the capacity of ESSs increases from 0.6 of the base value (S_1) to 1.8 of the base value (S_{10}). A further analysis is conducted to examine the impact of varying the participation rate of controllable consumers in the integrated DRP. This is carried out between S_4 and S_6 for a base capacity of ESSs. It is observed that the variation in these rates is reduced to 0.75% and 5.15% respectively. Conversely, the $\mathcal{DR}$ KPI has demonstrated a notable expansion of 60% when the participation rate of subscribers and the capacity of ESSs are augmented under S_{12} in comparison to S_4. Moreover, Fig. 8 illustrates the variations in the robustness degree of the independent PDN and DHN for each sample. A comparison of S_{12} and S_3 reveals that, despite both samples including controllable loads participating in the integrated DRP at an equivalent level, the capacity of the embedded ESSs in the test system in S_{12} is three times greater than that of S_3. This indicates that the test system's average robustness level is 10.6% higher in S_{12} than in S_3. Secondly, the fluctuations in the robustness level for S_{12} have reached the lowest possible level, and the changes in the 2^{nd} to 3^{rd} quartiles are less than 10%, demonstrating significantly enhanced stability compared to other samples. This improvement can be attributed to an increase in the capacity of backup resilience tools within the cascading failure framework, enabling a more effective system operator response to extreme critical events in the PDN. These results demonstrate how different technical backup resiliency tools mitigate the severity of cascading failures, directly supporting the practical implementation of the proposed resilient contingency management framework outlined in the stated objectives.

2) Empirical quantification of PDN-DHN resilience interdependence through statistical analysis: A comprehensive set of statistical analyses has been conducted for the purpose of quantifying the mutual resilience dependency between the PDN and DHN. These analyses were based on the values obtained for resilience KPIs under six contingency scenarios, which are reported in Table V. To validate the interdependency hypothesis, the Pearson correlation coefficient has been computed between each pair of resilience KPIs across the scenarios. Table VII shows the correlation metrics. The findings reveal that all observed correlations are statistically significant at the 0.03 level (p-value ≤ 0.03),

TABLE VII
PEARSON CORRELATION COEFFICIENTS BETWEEN RESILIENCE KPIS

	Correlation (r)	Significance (p-value)
$\mathcal{DR}$-$\mathcal{SD}$	-0.971	<0.01
$\mathcal{DR}$-$\mathcal{RR}$	-0.845	0.03
$\mathcal{SD}$-$\mathcal{RR}$	0.941	<0.01

with values exceeding 0.84. These results unmistakably signify a robust linear interdependence between the resilience of PDN and DHN, with the strength of this relationship increasing in the presence of backup tools. This finding serves to substantiate the hypothesis that disturbances and recoveries in PDN directly impact DHN resilience. Notably, the study's findings indicated negative correlations between $\mathcal{DR}$ KPI and two other resilience indicators, namely $\mathcal{SD}$ and $\mathcal{RR}$ KPIs. Although this inverse correlation may initially appear counterintuitive, it highlights the compensatory mechanisms inherent to the proposed framework. Specifically, as the magnitude of PDN disturbances increases, the DHN system, supported by distributed ESSs and integrated DRPs, exhibits reduced sensitivity and a faster autonomous recovery capability. This outcome signifies the hybrid PDN-DHN model's capacity for dynamic resilience and self-stabilizing tendencies when operated in a coordinated manner. Consequently, the negative correlation is indicative of a meticulously designed control structure that effectively mitigates cascading failures and restricts the propagation of faults. This finding underscores the multidimensional nature of resilience, indicating that an increase in perceived impact does not inherently lead to heightened vulnerability or delayed recovery. Instead, it underscores the robustness of the interdependent system when equipped with advanced flexibility mechanisms.

In addition, the normalized histograms depicting the calculated resilience KPI for Case 2 (a baseline benchmark lacking backup tools) and Case 6 are illustrated in Fig. 9. The distribution of each resilience KPI has been evaluated across a series of Monte Carlo simulations, with 100 iterations performed for each case. These histograms provide a visual representation of the impact of flexibility in the PDN on the DHN's resilient behavior. As the PDN degradation level increases and mitigation resources are lacking (Case 2), the $\mathcal{DR}$ KPI undergoes a significant decline, thus confirming the mutual dependency between the two. However, in Case 6, with the inclusion of ESSs and integrated DRP, the distributions shift rightward, accompanied by a reduction in variance (0.00032), signifying enhanced stability for the DHN during critical contingencies that transpired in PDNs. As demonstrated by the left-shifted, narrower histogram in Case 6, the recovery behavior of DHN is faster and more predictable, underscoring the effect of electricity-side resilience on the performance of thermal systems. These statistical findings lend credence to our hypothesis that the resilience of DHNs is not an isolated phenomenon but is tightly coupled with the operational state of PDNs. The observed interdependence is not only evident through qualitative assessments, such as recovery curves and energy shortages, but is now also substantiated by quantitative distributional analysis.

3) Dynamic assessment of resilience of test system under critical contingencies: This sub-section comprises an extensive series of experiments carried out using the RMS simulation function in the DIgSILENT PowerFactory software environment. The experiments are designed to demonstrate the influences of the synergistic development of power and heat networks on grid stability, voltage regulation, and current surges. The initial step in the process is to model the test system in PowerFactory, taking into account the resilience optimization results obtained in the presence of all local production units, conversion facilities, and ESSs. Subsequently, the dynamic characteristics of the interdependent

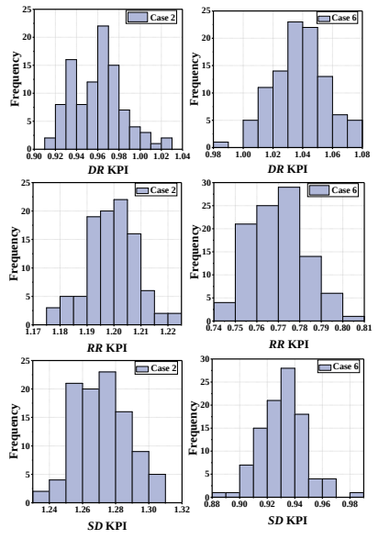

Fig. 9. Histograms of resilience KPIs for Case 2 vs Case 6.

PDN and DHN are evaluated by considering the critical N-1 contingency fault case. It was assumed that a three-phase short-circuit fault occurred at feeder $l5$, which represented the most critical point as expressed in Table III, during the peak load period (t=11:00) and was cleared after 0.2 seconds. Fig. 10 illustrates the voltage and positive sequence current magnitudes of the selected buses and feeders in the vicinity of critical points and coupling points of the PDN and DHN. As evidenced by the static studies, the ESSs played a pivotal role in enhancing the resilience of the interdependent PDN and DHN, even in the absence of these systems, the integrated DRP did not significantly impact the robustness of the integrated network, as illustrated in Fig. 8. To investigate this phenomenon, two distinct operational conditions have been employed for dynamic studies. As illustrated in Figs. 10(a) and 10(b), upon the occurrence of a fault, bus voltage magnitudes exhibit a pronounced decline. For instance, at bus 9, the voltage magnitude declines from a nominal 1 p.u. to 0.608 p.u. within the first 10 milliseconds. This rapid decline indicates a significant disturbance and challenges the PDN's voltage stability. The integration of BESS 3 demonstrates a notable enhancement in voltage stability. At bus 9, the voltage decline is only 0.65 p.u., a comparatively minor decline in comparison to the no-BESS scenario. This is attributed to the BESS's capacity to inject reactive power with alacrity in response to the fault. The extent of voltage sag is contingent upon the proximity to the fault location and the available capacity of BESSs. The voltage at bus 9 demonstrates a gradual recovery, rising to 1 p.u. over a period of 6.4 milliseconds. This slow recovery is attributed to the absence of additional reactive power support, which highlights the system's vulnerability to prolonged low-voltage conditions following fault clearance. In contrast with the presence of the BESS, the recovery of voltage at bus 9 is markedly faster, reaching 0.962 p.u. within 2.25 milliseconds and stabilizing at nominal voltage shortly thereafter. This quick stabilization is crucial for maintaining the reliability of sensitive loads connected to the bus. Similar trends are observed across other buses. As illustrated in Figs. 10(c) and 10(d), it can be observed that during the fault, line currents experience significant surges. For instance, the current through the line connecting bus 9 to bus 10 is reduced to 0.26 of its rated value in the absence of BESS 3. The presence of BESS 3 effectively mitigates the magnitude of fault current surges. For the same line, the current reduction is limited to 0.64 of the pre-fault value. Following the occurrence of the fault, the current decays more rapidly in the BESS-integrated scenario, returning to normal levels more quickly than in the no-BESS case. This rapid decay reduces the thermal and mechanical stress on the power system components. It can be concluded that

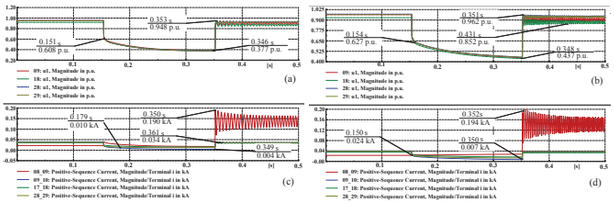

Fig. 10. Dynamic resilience response of interdependent PDNs and DHNs in the event of a tripping feeder $l5$ at hour 11:00: bus voltage magnitude (a) without consideration of BESS 3, and (b) in the presence of BESS 3; Line current magnitude (c) without consideration of BESS 3, and (d) in the presence of BESS 3.

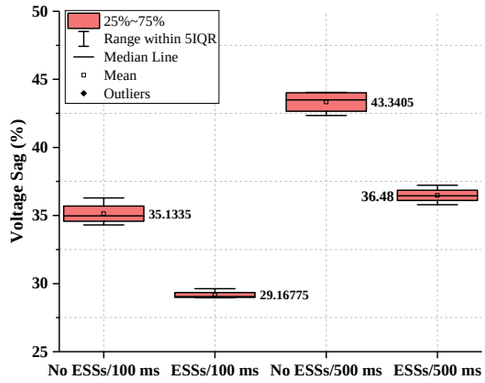

Fig. 11. Voltage sag distribution across all buses under a single-phase-to-ground fault for four scenarios.

the integration of PDN and DHN significantly affects the dynamic resiliency in fault conditions. Nevertheless, the deployment of large-scale backup resilient tools, such as BESSs, enhances voltage stability, reduces fault current surges, and mitigates thermal stress on PDN feeders.

To further enhance the robustness of the dynamic assessment and address a broader spectrum of realistic disturbances in distribution systems, a single-phase-to-ground fault, which represents over 70% of typical distribution network faults, is simulated at the most critical contingency point, i.e., feeder $l5$, during peak load time (t = 11:00). The present study considers four operational scenarios in order to evaluate the resilience of the system under different fault clearance times, i.e., 100 milliseconds (ms) and 500 ms, in the presence and absence of ESSs. A statistical evaluation of voltage sag at all buses is undertaken, encompassing both mean values and standard deviations. These evaluations are illustrated in Fig. 11. According to the results of the simulation, it has been demonstrated that the voltage stability of the system is significantly enhanced by the deployment of ESSs and the reduction of fault clearance times. Specifically, in the absence of ESSs, the average voltage sag across all buses reached 35.13% for a 100-ms fault clearance time, while increasing to 43.34% when the fault clearance was delayed to 500 ms. However, the presence of ESSs resulted in a significant reduction of the voltage sag, with the clearance decreasing to 29.17% for a 100 ms interval and 36.48% for a 500 ms interval. Furthermore, the standard deviation of voltage sag values across buses decreased considerably when ESSs were present. For instance, in a 100-ms scenario, the standard deviation dropped from 0.72 p.u. to 0.27 p.u., suggesting a more uniform voltage distribution across the network. From a dynamic response perspective, the network recovery time, defined as the duration for all bus voltages to return within 0.95–1.05 p.u., exhibited significant sensitivity to the presence of ESSs and the fault clearance time. In the absence of ESSs, the recovery time is found to be 56.4 ms for the 100 ms clearance, and it exhibited a marked increase to 195.4 ms for the 500 ms clearance. Conversely, the presence of ESSs resulted in a significant reduction in recovery times, measuring at 23.7 ms and 120.2 ms for the two scenarios, respectively. These findings substantiate the efficacy of ESSs in enhancing system voltage recovery and mitigating the impact of prolonged low-voltage conditions. The analysis indicates that single-phase-to-ground faults, while less severe compared to three-phase faults, can nevertheless generate significant voltage disturbances, especially in instances of delayed clearance. However, the coordinated integration of ESSs has been shown to enhance the dynamic resilience of the interdependent PDN and DHN. This enhancement is achieved by reducing voltage sags and accelerating recovery times under such faults. These results underscore the imperative for expeditious protection systems and adaptable distributed energy resources to ensure stability in the presence of asymmetric faults.

C. Technical and operational limitations: Design trade-offs and implementation considerations

The proposed framework for an integrated PDN-DHN assessment of resilience has been meticulously crafted with a pronounced emphasis on practical feasibility, computational scalability, and industrial applicability. Despite the rigorous efforts undertaken to devise a robust and implementable strategy, it is imperative to acknowledge the existence of certain technical and operational limitations. The preponderance of these limitations can be attributed to the necessity of making informed trade-offs to ensure model transparency, modularity, and simulation tractability. It is crucial to note that these deviations are not merely oversights but rather deliberate modeling choices made after a thorough evaluation of the complexity-performance trade space.

A primary strength of this study is its two-phase framework, which captures both the static (topology-driven) and dynamic (time-dependent) aspects of resilience across interdependent energy infrastructures. In contrast to the numerous extant studies that have focused exclusively on topological robustness or steady-state indicators, our approach enables the quantification of the temporal evolution of dynamic restoration profiles under resource constraints. Nonetheless, the simplification of hydraulic transients in DHNs along with the assumption of rapid control actions may not entirely capture the slower thermodynamic inertia observed in low-temperature systems. The implementation of a CF–VT control strategy for the DHN facilitates compatibility with conventional district heating systems and mitigates the hydraulic modeling burden. This assumption is indicative of the prevailing infrastructure in numerous metropolitan areas where CF–VT continues to predominate. However, this limitation can be addressed by integrating detailed dynamic models in future developments. In emerging smart heating systems employing variable flow or intelligent control (e.g., CT–VF, VF–VT), more responsive strategies may yield better resilience under extreme events. Although advanced heating control schemes, such as CT–VF and VF–VT, are gaining popularity in modern DHNs, their integration introduces significant nonlinearities and control-optimization coupling. These phenomena result in increased computational burden and affect model convexity. Consequently, the present utilization of CF–VT furnishes a substantial yet manageable depiction congruent with pragmatic DHN implementations, thereby establishing the foundation for prospective integration of intelligent and adaptive control models. The expansion of the model to accommodate such strategies is a possibility; however, it would require real-time flow-temperature coupling, actuator dynamics, and data-driven learning, which are beyond the current model's static scope. Subsequent endeavors will incorporate these dynamics to augment the engineering relevance of the model.

Furthermore, a secondary objective in the design process was to ascertain the feasibility of the proposed strategy

for implementation by utility operators, with the aim of leveraging existing infrastructure and data resources. However, in more sophisticated scenarios, such as predictive control, dynamic dispatch, or cyber-physical coordination, additional real-time metering and sensor deployment may be required. Notwithstanding, the proposed model maintains a high degree of fidelity for real-world applications. The aforementioned strategy was meticulously formulated to address the disparity between academic modeling and operational usability by integrating static and dynamic resilience analysis, optimizing resource allocation, and reflecting real-world infrastructure constraints. Moreover, regarding scalability, the convex MILP formulation of the proposed framework guarantees global convergence while remaining computationally efficient. This property ensures that the methodology is inherently scalable to large-scale urban integrated PDN–DHN systems without loss of accuracy or tractability. In practice, the case studies conducted as part of this work were all solved with a zero optimality gap, and within an acceptable computation time (i.e., less than 1 minute per scenario on a standard workstation). Complementary dynamic simulations were implemented in DIgSILENT, which is widely used for industrial-scale systems, further confirming the practical applicability of the framework to real-world urban networks.

V. Conclusion

In response to the growing need for integrated resilience analysis of interdependent energy infrastructures, this paper unveiled a contingency multi-criteria decision-making analytical framework. The analytical framework was tailored to quantify the cascading effects of critical power feeder outages on the operation of DHNs and to assess the bidirectional resilience interdependence between PDNs and DHNs. By incorporating the SECA method, the framework effectively identified high-impact N-1 and N-k contingency scenarios, and the subsequent ranking of vulnerable feeders based on multi-phase interdependency indicators. To evaluate system performance under such contingencies, a cascading failure analysis model was developed, capturing the energy-serving capacity degradation of interlinked PDNs and DHNs in the presence or absence of resilience backup tools. A series of static and dynamic studies were conducted on a modified IEEE 33-bus PDN supplying PtH units in a 32-node DHN. The following key findings were demonstrated: The deployment of ESSs, in conjunction with the effective management of controllable subscribers, resulted in a substantial reduction in PtH unit interruptions and the subsequent heat shortages. In the most critical N-k contingency scenarios, the sensitivity of the DHN to PDN disruptions decreased by 21.69% compared to a baseline case without backup resilience tools. Furthermore, the optimal coordination of DRPs and ESSs significantly enhanced system robustness, reducing the downtime of non-critical customers by approximately 92.42% and improving the withstand capability of the integrated PDN-DHN system in the event of critical N-k contingencies.

This study delineates avenues for future research, with a particular focus on the incorporation of advanced heating controls, cyber-physical resilience interactions, and data-driven decision support modules that exhibit scalability in accordance with the demands of the system. In addition, future research may extend the proposed framework beyond equipment outages to explicitly account for external disruptions such as weather-induced feeder failures, natural disasters, or long-term gas supply interruptions. Incorporating these exogenous events would further enhance the applicability of the framework in capturing cross-sectoral resilience challenges under realistic large-scale contingency scenarios.

Acknowledgments

The authors acknowledge support of the "Distributed control architecture for resilient operation of combined distribution and district heating networks" project funded by the Scientific and Technological Research Council of Turkey (TUBITAK) under Grant No. 121C413. The work of Prof. Erdinç was supported by "Versatile Energy Sources Enhancing Resiliency for Integrated PowER and Gas Infrastructure (VESPER)" project funded by Fundacao para a Ciencia e a Tecnologia (FCT), Science Academy Young Scientists Award Program (BAGEP), Turkey, and TUBITAK 100^{th} year Science Encouragement Award. The work of J.P.S. Catalão was supported by the EU Horizon Europe Programme under GA ID: 101160614 (EU-DREAM Project, DOI: 10.3030/101160614), and also by FEDER (COMPETE2030) and FCT through MPr-2023-12 (INVINCIBLE Project, Ref. COMPETE2030-FEDER-00883700).

References

[1] Y. Cao, W. Wei, L. Wu, S. Mei, M. Shahidehpour, and Z. Li, "Decentralized operation of interdependent power distribution network and district heating network: A market-driven approach," *IEEE Transactions on Smart Grid*, vol. 10, no. 5, pp. 5374–5385, 2019.

[2] M. Z. Oskouei, B. Mohammadi-Ivatloo, M. Abapour, M. Shafiee, and A. Anvari-Moghaddam, "Strategic operation of a virtual energy hub with the provision of advanced ancillary services in industrial parks," *IEEE Transactions on Sustainable Energy*, vol. 12, no. 4, pp. 2062–2073, 2021.

[3] M. Z. Oskouei, F. Gülşen Erdinç, and O. Erdinç, "Analysis of power-to-heat units penetration effect on dynamic behavior of power distribution grids," in *2024 6th Global Power, Energy and Communication Conference (GPECOM)*, 2024, pp. 524–529.

[4] "Cybersecurity and infrastructure security agency (CISA), [online]. available at: https://www.cisa.gov/news-events/ics-alerts/ir-alert-h-16-056-01," 2021.

[5] M. Zare Oskouei, H. Mehrjerdi, D. Babazadeh, P. Teimourzadeh Baboli, C. Becker, and P. Palensky, "Resilience-oriented operation of power systems: Hierarchical partitioning-based approach," *Applied Energy*, vol. 312, p. 118721, 2022.

[6] E. A. Martínez Ceseña and P. Mancarella, "Energy systems integration in smart districts: Robust optimisation of multi-energy flows in integrated electricity, heat and gas networks," *IEEE Transactions on Smart Grid*, vol. 10, no. 1, pp. 1122–1131, 2019.

[7] M. Yan, Y. He, M. Shahidehpour, X. Ai, Z. Li, and J. Wen, "Coordinated regional-district operation of integrated energy systems for resilience enhancement in natural disasters," *IEEE Transactions on Smart Grid*, vol. 10, no. 5, pp. 4881–4892, 2019.

[8] Y. Chen, J. Wang, R. Bo, C. Gu, and Q. Li, "Risk-averse scheduling of integrated electricity-heat systems considering multi-energy network operations for resilience enhancement against contingencies," *International Journal of Electrical Power Energy Systems*, vol. 153, p. 109313, 2023.

[9] Y. Zhou, Z. Wei, M. Shahidehpour, and S. Chen, "Distributionally robust resilient operation of integrated energy systems using moment and wasserstein metric for contingencies," *IEEE Transactions on Power Systems*, vol. 36, no. 4, pp. 3574–3584, 2021.

[10] H. Zhang, P. Wang, S. Yao, X. Liu, and T. Zhao, "Resilience assessment of interdependent energy systems under hurricanes," *IEEE Transactions on Power Systems*, vol. 35, no. 5, pp. 3682–3694, 2020.

[11] S. Lu, Y. Li, S. Ding, W. Gu, Y. Xu, and M. Song, "Combined electrical and heat load restoration based on bi-objective distributionally robust optimization," *IEEE Transactions on Industrial Informatics*, vol. 19, no. 8, pp. 9239–9252, 2023.

[12] H. Masrur, M. M. Gamil, M. R. Islam, K. M. Muttaqi, M. S. H. Lipu, and T. Senjyu, "An optimized and outage-resilient energy management framework for multicarrier energy microgrids integrating demand response," *IEEE Transactions on Industry Applications*, vol. 58, no. 3, pp. 4171–4180, 2022.

[13] K. Wang, Y. Xue, Q. Guo, M. Shahidehpour, Q. Zhou, B. Wang, and H. Sun, "A coordinated reconfiguration strategy for multi-stage resilience enhancement in integrated power distribution and heating networks," *IEEE Transactions on Smart Grid*, vol. 14, no. 4, pp. 2709–2722, 2023.

[14] Y. Zhou, X. Li, H. Han, Z. Wei, H. Zang, G. Sun, and S. Chen, "Resilience-oriented planning of integrated electricity and heat systems: A stochastic distributionally robust optimization approach," *Applied Energy*, vol. 353, p. 122053, 2024.

[15] T. Jiang, T. Sun, G. Liu, X. Li, R. Zhang, and F. Li, "Resilience evaluation and enhancement for island city integrated energy systems," *IEEE Transactions on Smart Grid*, vol. 13, no. 4, pp. 2744–2760, 2022.

[16] Q. Sun, Z. Wu, W. Gu, X.-P. Zhang, Y. Lu, P. Liu, S. Lu, and H. Qiu, "Resilience assessment for integrated energy system considering gas-thermal inertia and system interdependency," *IEEE Transactions on Smart Grid*, vol. 15, no. 2, pp. 1509–1524, 2024.

[17] S. Lei, C. Chen, Y. Song, and Y. Hou, "Radiality constraints for resilient reconfiguration of distribution systems: Formulation and application to microgrid formation," *IEEE Transactions on Smart Grid*, vol. 11, no. 5, pp. 3944–3956, 2020.

[18] M. Z. Oskouei, A. K. Erenoğlu, and O. ErdıNç, "Identification of critical feeders in integrated electricity and district heating networks for decentralized implementation of proactive schemes," in *2024 IEEE International Conference on Industrial Technology (ICIT)*, 2024, pp. 1–6.
[19] M. Zare Oskouei and G. B. Gharehpetian, "Flexibility enhancement of multi-district discos considering a trade-off between congestion and extractable reserve capacity from virtual energy storage systems," *Applied Energy*, vol. 353, p. 122181, 2024.
[20] B. Vatandoust, A. Ahmadian, M. A. Golkar, A. Elkamel, A. Almansoori, and M. Ghaljehei, "Risk-averse optimal bidding of electric vehicles and energy storage aggregator in day-ahead frequency regulation market," *IEEE Transactions on Power Systems*, vol. 34, no. 3, pp. 2036–2047, 2019.
[21] H. Tian, H. Zhao, C. Liu, J. Chen, Q. Wu, and V. Terzija, "A dual-driven linear modeling approach for multiple energy flow calculation in electricity–heat system," *Applied Energy*, vol. 314, p. 118872, 2022.
[22] Y. Zhou, M. Shahidehpour, Z. Wei, Z. Li, G. Sun, and S. Chen, "Distributionally robust unit commitment in coordinated electricity and district heating networks," *IEEE Transactions on Power Systems*, vol. 35, no. 3, pp. 2155–2166, 2020.
[23] X. Liu, J. Wu, N. Jenkins, and A. Bagdanavicius, "Combined analysis of electricity and heat networks," *Applied Energy*, vol. 162, pp. 1238–1250, 2016.
[24] M. Z. Oskouei and H. Mehrjerdi, "Multi-stage proactive scheduling of strategic discos in mutual interaction with cloud energy storage and deferrable loads," *IEEE Transactions on Sustainable Energy*, vol. 14, no. 3, pp. 1411–1424, 2023.

Morteza Zare Oskouei was born in Osku, Iran, in 1991. He received his Ph.D. degree in electrical engineering from the University of Tabriz, Iran, in 2021 (all with honors). He has worked as a postdoctoral researcher at Qatar University, Doha, Qatar, from October 2021 to September 2022. After that, he joined the Tabriz University of Technology, Tabriz, IRAN, as an Assistant Professor at the Faculty of Electrical and Computer Engineering. His main areas of interest are renewable-dominated integrated energy systems, energy systems flexibility and resiliency, machine learning, demand response programs, virtual energy storage systems, and energy markets. He has strong professional skills in GAMS software and DIgSILENT PowerFactory.

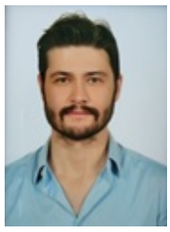

Tayfur Gökçek received the B.Sc., M. Sc. and Ph.D. degrees from Yildiz Technical University (YTU), Istanbul, Turkey, in January 2019, June 2021, and January 2025, respectively. Until September 2019, he was in the private sector in wind turbine installation as a site engineer. In February 2020, he joined the Department of Electrical Engineering, YTU as a research assistant. He is currently working as an Assistant Professor in YTU Clean Energy Technologies Institute. He continues his research on various optimization problems across all levels of electrical power systems, including smart homes, electric vehicles/ships, energy trading, energy markets, and coordinated grid operation. In addition to these, he is also actively involved in experimental studies. He has taken part as a scholar, researcher, and consultant in numerous projects supported by different funding bodies.

Ayşe Kübra Erenoğlu (Senior Member, IEEE) received the B.Sc., M.Sc., and Ph.D. degrees in Electrical Engineering from Yıldız Technical University (YTU), Istanbul, Turkey, in 2016, 2018, and 2021, respectively. In April 2017, she joined the Department of Electrical Engineering at Yıldız Technical University as a Research Assistant. In November 2022, she was appointed as an Assistant Professor in the Department of Electrical and Electronics Engineering at Fatih Sultan Mehmet Vakıf University. She is currently working as an Assistant Professor in the Department of Electrical Engineering at Yıldız Technical University and serves as the University–Industry Collaboration Coordinator at the Institute of Clean Energy Technologies. Dr. Erenoğlu is actively engaged in the IEEE community. She is the elected Chair of the IEEE Power and Energy Society (PES) Turkey Chapter. She has contributed as a Technical Program Committee Member in IEEE co-sponsored conferences. Her research interests include power system resilience, smart grid applications, renewable energy integration, and electric vehicles.

Ozan Erdinç received his BSc, MSc, and PhD degrees from Yildiz Technical University (YTU), Turkey, in 2007, 2009, and 2012, respectively. Until May 2013, he worked in industry in various positions related to electrical installations and renewable energy investments. In June 2013, he became a Postdoctoral Fellow in Portugal under the EU-FP7 SINGULAR Project. He later joined the Department of Electrical Engineering at YTU, earning the title of Associate Professor in 2016 and Full Professor in 2021. He has served as Director of YTU Energy Application and Research Center, Head of YTU IT Department, Head of the Alternative Energy Based Electric Systems Division, and IEEE Power and Energy Society (PES) Turkey Chapter Chair (2019–2023). Since October 2024, he has been working as a researcher at the Faculty of Engineering, University of Porto, leading the FCT-funded "VESPER" project. He is also a Board Member of the YTU Clean Energy Technologies Institute and the Electrical Installation Engineers Association of Türkiye.

Prof. Erdinç is the sole editor of Optimization in Renewable Energy Systems (Butterworth-Heinemann, 2017) and co-editor of Pathways to a Smarter Power System (Academic Press, 2019). He has authored over 150 international publications,.He has led or consulted on 20 projects with budgets exceeding 15 million EUR in total. He has served in various roles at IEEE-sponsored conferences, delivered keynote speeches and invited lectures internationally, and received prestigious awards including TUBA GEBIP (2020), IEEE Turkiye Section Research Encouragement Award (2021), TUBITAK Research Encouragement Award (2023), and BAGEP (2024). A Senior Member of IEEE, he has held editorial roles for leading journals such as IEEE Transactions on Sustainable Energy, and IEEE Transactions on Intelligent Transportation Systems.

João P. S. Catalão (Fellow, IEEE) is a Full Professor ("Professor Catedrático") at the Faculty of Engineering of the University of Porto, Portugal. He was a Highly Cited Researcher in the field of Engineering in 2023. He is among the Top 2% of Scientists, since 2019, and a Best Scientist 2022-2025 in Research.com. He was the Primary Coordinator of the 5.2-million-euro FP7-EU project SiNGULAR, 2012-2015. Currently, he is the Primary Coordinator of the 4.5-million-euro Horizon-EU project EU-DREAM, 2024-2027. He has coauthored more than 500 journal publications, with an h-index of 108 and more than 43,000 citations (according to Google Scholar), having supervised more than 140 researchers (post-docs, Ph.D. and M.Sc. students, and other students with project grants). He was the General Chair of SEST 2019 (technically co-sponsored by IEEE), after being the inaugural Technical Chair and co-founder of SEST 2018. He was the Editor of two CRC Press Books: "Electric Power Systems: Advanced Forecasting Techniques and Optimal Generation Scheduling" (2012) and "Smart and Sustainable Power Systems: Operations, Planning and Economics of Insular Electricity Grids" (2015). He is a Senior Editor of the IEEE TRANSACTIONS ON NEURAL NETWORKS AND LEARNING SYSTEMS, a Senior Editor of the IEEE TRANSACTIONS ON SYSTEMS, MAN, AND CYBERNETICS: SYSTEMS, and a Senior Associate Editor of the IEEE TRANSACTIONS ON CIRCUITS AND SYSTEMS PART II: EXPRESS BRIEFS. He was an IEEE CIS Fellows Committee Member in 2022-2024 (three consecutive years). He was elected Full Member of Sigma Xi, The Scientific Research Honor Society, in 2023. He was recognized as an Outstanding Associate Editor 2023 of the IEEE TRANSACTIONS ON EMERGING TOPICS IN COMPUTATIONAL INTELLIGENCE, an Outstanding Associate Editor 2021 of the IEEE TRANSACTIONS ON POWER SYSTEMS, and an Outstanding Senior Associate Editor 2020 of the IEEE TRANSACTIONS ON SMART GRID. Furthermore, he has won 5 Best Paper Awards at IEEE Conferences. His research interests include power system operations and planning, power system economics and electricity markets, distributed renewable generation, demand response, smart grid, and multi-energy carriers.